

Review

Architecture Evolution of Different Nanoparticles Types: Relationship between the Structure and Functional Properties of Catalysts for PEMFC

Sergey Belenov ^{*} , Anastasia Alekseenko , Angelina Pavlets, Alina Nevelskaya and Maria Danilenko 

Chemistry Faculty, Southern Federal University, 344090 Rostov-on-Don, Russia; aalekseenko@sfedu.ru (A.A.); pavlec@sfedu.ru (A.P.); nevelskaya@sfedu.ru (A.N.); mdanilenko@sfedu.ru (M.D.)

* Correspondence: serg1986chem@mail.ru

Abstract: This review considers the features of the catalysts with different nanoparticle structures architecture transformation under the various pre-treatment types. Based on the results of the publications analysis, it can be concluded that the chemical or electrochemical activation of bimetallic catalysts has a significant effect on their composition, microstructure, and catalytic activity in the oxygen reduction reaction. The stage of electrochemical activation is recommended for use as a mandatory catalyst pre-treatment to obtain highly active de-alloyed materials. The literature is studied, which covers possible variants of the structural modification under the influence of thermal treatment under different processing conditions. Additionally, based on the literature data analysis, recommendations are given for the thermal treatment of catalysts alloyed with various d-metals.

Keywords: pt-based electrocatalysts; bimetallic nanoparticles; alloy structure; core-shell; intermetallic structure; acid treatment; electrochemical activation; thermal treatment; oxygen reduction reaction; stability



Citation: Belenov, S.; Alekseenko, A.; Pavlets, A.; Nevelskaya, A.; Danilenko, M. Architecture Evolution of Different Nanoparticles Types: Relationship between the Structure and Functional Properties of Catalysts for PEMFC. *Catalysts* **2022**, *12*, 638. <https://doi.org/10.3390/catal12060638>

Academic Editor: Yongjun Feng

Received: 1 May 2022

Accepted: 8 June 2022

Published: 10 June 2022

Publisher's Note: MDPI stays neutral with regard to jurisdictional claims in published maps and institutional affiliations.



Copyright: © 2022 by the authors. Licensee MDPI, Basel, Switzerland. This article is an open access article distributed under the terms and conditions of the Creative Commons Attribution (CC BY) license (<https://creativecommons.org/licenses/by/4.0/>).

1. Introduction

To create highly efficient low-temperature fuel cells (FC), it is necessary to improve the specific characteristics of platinum-containing catalysts, which are the most important component of FC [1–3]. The use of Pt-based nanoparticles (NPs) with different compositions and structures deposited on a highly dispersed carbon support makes it possible to reduce the content of noble metals in the material while increasing the activity and stability of the catalyst [4–7]. Note that the morphology of bimetallic catalysts is determined by the shape, composition of the metal component, architecture and size of metal NPs, as well as their spatial distribution on the support surface. All these factors have a vital impact on the catalyst's activity in the oxygen reduction reaction (ORR) and their stability [8,9].

It is well known that platinum doping with some d-metals increases the catalyst activity due to a number of effects, as follows: (1) a change in the electronic structure of the metal; (2) a decrease in the interatomic distance in the metal crystal lattice, which contributes to the dissociative adsorption of oxygen molecules; (3) a change in the surface oxides' composition and an increase in the corrosion resistance of the alloy in comparison to pure Pt [10–13]. Note that bimetallic systems have several disadvantages, and the main one is the tendency to dissolve the base component of the catalyst during the fuel cell operation [14,15]. To solve this problem, materials with a special architecture of bimetallic NPs are obtained: core-shell [4,6,16,17], gradient [18,19], onion structure [20,21], hollow [4]. In NPs with this structure, the platinum layer is assumed to be on the NP surface and reliably protects the alloying component from dissolution during catalyst operation [16,22,23]. There are a few works that show the effect of the platinum shell thickness on the activity and stability of NPs [24]. In the studies of recent years, it has been established that when forming a plurality of bimetallic NPs on the carbon surface, it is not

possible to provide the desired architecture for all NPs [19,25,26]. In addition, the platinum shell, as a rule, does not provide complete protection of the core component from dissolution in the electrolyte [27]. To solve this problem, various types of catalyst treatment are used, which can be divided into acid treatment and heat treatment. Even though there are a few reviews on the latest advances in the field of platinum-containing catalysts for proton exchange membrane fuel cells (PEMFC) [4,28] including the composition and structure of bimetallic NPs [4,6,16], there are very few reviews on catalyst pre-treatment. Note the presence of a review (2007) on the heat treatment of materials, which does not consider the effect of heat treatment on the NPs architecture [29]. In most studies, the treatment of catalysts is considered one of the synthesis stages and is not always described in detail. At the same time, it is obvious that the treatment conditions have a significant effect on the size and architecture of platinum-containing NPs and, therefore, on the functional characteristics of the catalysts. Therefore, the current goal of this work is to systematize and analyze the latest literature data on various types of pre-treatment of Pt-based materials. An analysis of the pre-treatment conditions' influence on the structure and functional characteristics of Pt-based catalysts will make it possible to formulate recommendations on the optimal parameters of catalyst treatment to increase their activity and stability, depending on their composition and structure.

2. De-Alloyed Treatment

It is known that the composition of bimetallic NPs changes during their operation, resulting in the selective dissolution of the alloying component atoms, firstly from the NPs surface layer [14,15]. When conducting measurements in an electrochemical cell in the presence of a substantive amount of a liquid electrolyte, the concentration of cations M^{z+} in the solution is low and cannot significantly affect the characteristics of the electrode. During the catalyst operation in the membrane-electrode assembly (MEA), the transition of the alloying cations into the electrolyte can lead to the substitution of protons in the sulfo-groups of proton-conducting polymer to metal [14,15]. Such poisoning of the polymer will impede the transport of protons and reduce the conductivity of the polymer membrane in the FC [14]. This determined the direction of many studies related to form bimetallic NPs, which initially have an uneven structure of core (alloying metal)–shell (Pt) [4,6,16–19]. In several works, it was noted that in bimetallic NPs with a core–shell and a gradient structure, the positive effect of the core component on the catalytic activity of platinum can be preserved [4,6,16–19].

Many recent publications have noted that catalysts based on de-alloyed PtM (M = Cu, Co, Ni) NPs containing a relatively small amount of tightly bound base metal are promising for use in MEA of fuel cells. It is very problematic to directly synthesize such catalysts that combine high activity in the ORR and a low content of the alloying component. They can be, however, obtained by the pre-treatment of PtM_x/C (x > 1) materials rich in d-metal in an acidic medium. In this case, it is important to make sure that, firstly, the preferential dissolution of the alloying metal atoms will make it possible to form a secondary-formed Pt shell that protects the internal M atoms from dissolution. Secondly, it is necessary to determine whether these de-alloyed PtM_{x-y}/C catalysts maintain high stability and activity in the ORR.

The issues of using de-alloying to obtain functional materials are widely considered in reviews of recent years [30,31]. However, in this case, bulk composites are studied, and de-alloyed treatment is used to obtain bulk nanoporous materials, including those exhibiting catalytic activity.

At the same time, our review considers the use of this process only for objects that act as a catalyst for fuel cells, and it is not necessarily true that de-alloying leads to nanoporosity. Let us consider the effect of de-alloyed pretreatment on the characteristics of bimetallic catalysts.

There are two bimetallic catalyst de-alloyed pre-treatments. The first treatment type, which consists of aging in acids, is called acid treatment (Table 1). The second pre-treatment

type for obtaining de-alloyed NPs is called electrochemical activation (electrochemical de-alloying) and is carried out by holding the material in an acidic medium while changing the potential (Table 2). Each of these approaches allows one to vary the treatment conditions, thereby influencing the structural and morphological characteristics of the obtained de-alloyed materials (Figure 1, Tables 1 and 2).

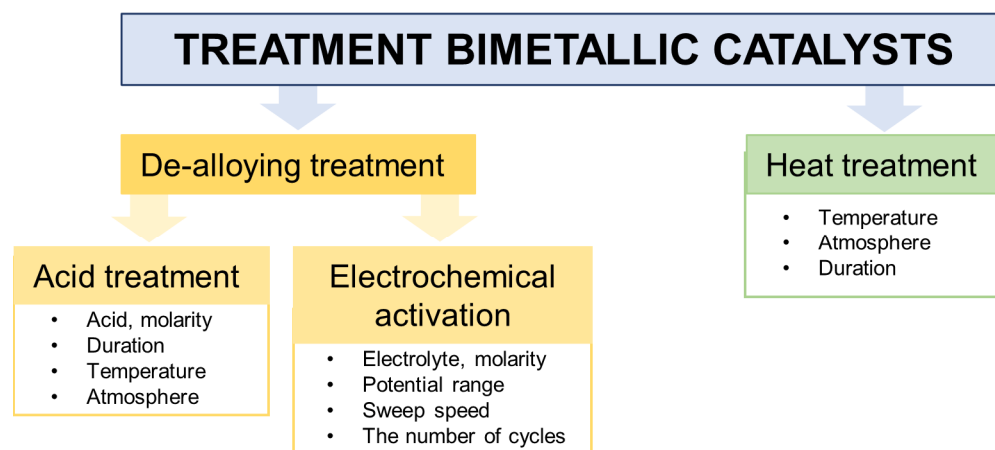


Figure 1. Schematic representation of treatment types of bimetallic catalysts. The parameters that can be varied during processing are indicated.

Note that a feature of bimetallic catalysts obtained by synthesis without the use of additional stabilizing agents is the presence in the final product particles that are different in composition, structure (M, PtM, Pt), and size. During acid treatment [32–45] and electrochemical de-alloying [46–60], bimetallic NPs can undergo various transformations depending on their composition and structure. Thus, a separately distributed component in the form of an oxide of an alloying metal completely dissolves upon contact with an acid (Figure 2a,k).

In a few studies, including those of our team, it was noted that the creation of catalysts containing bimetallic NPs with a certain idealized structure is a complex and apparently impossible task (Figure 2b,d) [14,15,32]. During the synthesis of bimetallic catalysts, the resulting NPs are most often characterized not only by different size, but also by different composition. Bimetallic particles with different structures (solid solution, core–shell, gradient) obtained by wet synthesis methods are characterized by the presence of an alloying component on the surface. During the acid treatment of such bimetallic materials, the NPs are transformed into secondary structures with the prevailing segregation of platinum atoms in the surface layer and with the formation of a Pt-skin (Figure 2c,e,f,j–n,p,q). Additionally, the Pt-shell, as a rule, does not provide complete protection of the component that makes up the core from dissolution in the electrolyte. In this case, the process of significant washing out of the alloying component and the formation of void NPs (o) take place.

2.1. Acid Treatment

Bimetallic catalyst pre-treatment by holding in acids is a promising and easily scalable way to obtain de-alloyed materials. Both materials obtained by chemical reduction in the liquid phase and catalysts obtained after preliminary annealing with additional reduction are subjected to acid treatment to ensure the complete alloying of the components [33–35]. With this type of treatment, the composition [36] and concentration of acid [36–38], as well as time of treatment [18] and atmosphere [39,40], can be varied.

The authors [33,34,38,39,41] note during chemical treatment that the bimetallic particles average size decreases by 3–70%.

Table 1. Structural and electrochemical characteristics of acid-treated bimetallic catalysts.

Sample	Initial Composition	Pt [wt. %]	Composition after Acid Treatment	Treatment Conditions			Electrochemical Characteristics		Ref.	
				Acid, Molarity	Duration	Temperature	Features	ESA, m^2g^{-1} (Pt)		Activity in ORR, A mg^{-1} (Pt)
PtNi/C	Pt ₂₅ Ni ₇₅	28	Pt ₅₅ Ni ₄₅	0.5 M H ₂ SO ₄	24 h	room	0.5 g of catalyst—100 mL of acid with stirring, air atmosphere	30	740	[39]
PtNi/C	PtNi ₃	25	Pt ₃₄ Ni ₆₆				0.5 g of catalyst—100 mL of acid with stirring, N ₂	28	760	
PtCu/C	Pt _{0.3} Cu	-	Pt _{1.8} Cu	1 M HNO ₃	2 days	room	-	50	290	[33]
PtCu/C	PtCu _{0.84}	14.8	PtCu _{0.62}	1.5 M H ₂ SO ₄	3 h	room	-	57.5	200	[34]
PtCu/C	PtCu _{2.86}	10.12	PtCu _{0.76}					22.8	501	
PtCu/C	PtCu _{4.65}	7.2	PtCu _{0.53}					46.7	407	
Cu@Pt/C	Pt ₇₈ Cu ₂₂	-	Pt ₈₉ Cu ₁₁	1 M HNO ₃	2 h	room	Accompanied by ultrasonic processing	62.86	230	[23]
Hollow PtNi/C	Pt ₅₀ Ni ₅₀	-	Pt ₉₂ Ni ₈	1 M H ₂ SO ₄	22 h	20 °C	-	-	500	[42]
Hollow PtCo/C	Pt ₈₁ Co _{19±5}	-	Pt ₈₁ Co _{4.1±3}	1 M H ₂ SO ₄	24 h	room	-	-	150 ($\mu\text{A cm}^{-2}$)	[43]
PtCu/C	PtCu _{2.20}	14	PtCu _{0.76}	1 M HNO ₃	6 h	room	-	103	200	[36]
Nanoporous PtNi/C	Pt _{0.36} Ni _{0.64}	-	Pt _{0.79} Ni _{0.21}	Conc. HNO ₃	1 min	room	Particles without a support were processed under the influence of ultrasound	85.6	-	[41]
PtCu/C	PtCu _{0.67}	22.2	PtCu _{0.36}	1 M HNO ₃	3 h	room	-	48	332	[45]
PtCu/C	Pt ₁₉ Cu ₈₁	6.5	Pt ₄₇ Cu ₅₃	1 M CH ₃ COOH	2 h	room	4-fold acid washing with CO atmosphere for 30 min per stage	91	1870	[40]
PtFe/C	-	-	Pt ₈₄ Fe ₁₆	0.5 M H ₂ SO ₄	12 h	60 °C	-	54	159	[35]
PtNi/Pt	-	2-15	-	0.01 M HCl	1 h	room	-	52.65	800	[37]

Table 2. Structural and electrochemical characteristics of bimetallic catalysts after electrochemical activation.

Sample	Initial Composition	Pt [wt. %]	Composition after Activation	Treatment Conditions				Electrochemical Characteristics			Ref.
				Electrolyte, Molarity	Potential Range	Sweep Speed, mV s^{-1}	The Number of Cycles	ESA, $\text{m}^2 \text{g}^{-1}$ (Pt)	Activity, MA A mg^{-1} (Pt)	Activity, SA mA cm^{-2}	
Nanowire PtCu/C	Pt/Cu 0.59	20	Pt/Cu 1.43	0.5 M H_2SO_4 or 0.1 M HClO_4	-0.2 to 0.9 V vs. Ag/AgCl	400	400	63.5	3.15	-	[32]
PtCu/C	1:3, $\text{Pt}_{25}\text{Cu}_{75}$	22	($\text{Pt}_{79}\text{Cu}_{21}$) pure surface Pt ($\text{Pt}_{93}\text{Cu}_7$)	0.1 M HClO_4	0.06 to 1.2 V vs. RHE	1000	200	89	0.52	0.5	[46]
PtCu/CA	PtCu	20	-	0.1 M HClO_4	0 to 1.1 V vs. RHE	50	300	72.4	0.054	0.075	[52]
PtCu/C	PtCu	21	-	0.1 M HClO_4	0 to 1.1 V vs. RHE	50	300	46.3	0.113	0.244	
PtNi/C	Ni:Pt (72:28) 1:3 Pt: Ni	-	Ni:Pt (22:78)	0.1M HClO_4	Step 1: 0.05 to 1.2 V vs. RHE	0.5	200	-	-	2.6	[53]
					Step 2: 0.06 to 1.2 V vs. RHE	100	3				
PtNi/C	$\text{Ni}_{75}\text{Pt}_{25}$	-	-	0.1M H_2SO_4	0.05 to 1.2 V vs. RHE	250	>50	41	$1.16 \pm 0.035 \text{ mA } \mu\text{gPt}^{-1}$	2.98 ± 0.12	[54]
PtCu/C	Cu_3Pt	26	56% Cu	0.1 M HClO_4	0.05 to 1.2 V vs. RHE	200	500	23	0.58	2.5	
PtCu/C	Cu_3Pt	26	80% Cu	0.1 M HClO_4	holding the potential at 1.2 V (15 min or 2 h)	-	-	32	0.77	2.4	[55]
PtCo/C	$\text{Pt}_{37\pm 2}\text{Co}_{63\pm 2}$	-	$\text{Pt}_{80\pm 2}\text{Co}_{20\pm 2}$	0.1 M HClO_4	0.06 to 1.0 V vs. RHE	100	3	45	0.38	0.804	[59]
						500	200				
						100	3				
PtCu/C	$\text{Pt}_{35\pm 2}\text{Cu}_{65\pm 2}$	-	$\text{Pt}_{65\pm 2}\text{Cu}_{35\pm 2}$	0.1 M HClO_4	0.06 to 1.0 V vs. RHE	100	3	47	0.41	0.873	
						500	200				
						100	3				
PtCu/C				0.1 M HClO_4	0.05 to 1.35 V vs. RHE	300				[60]	

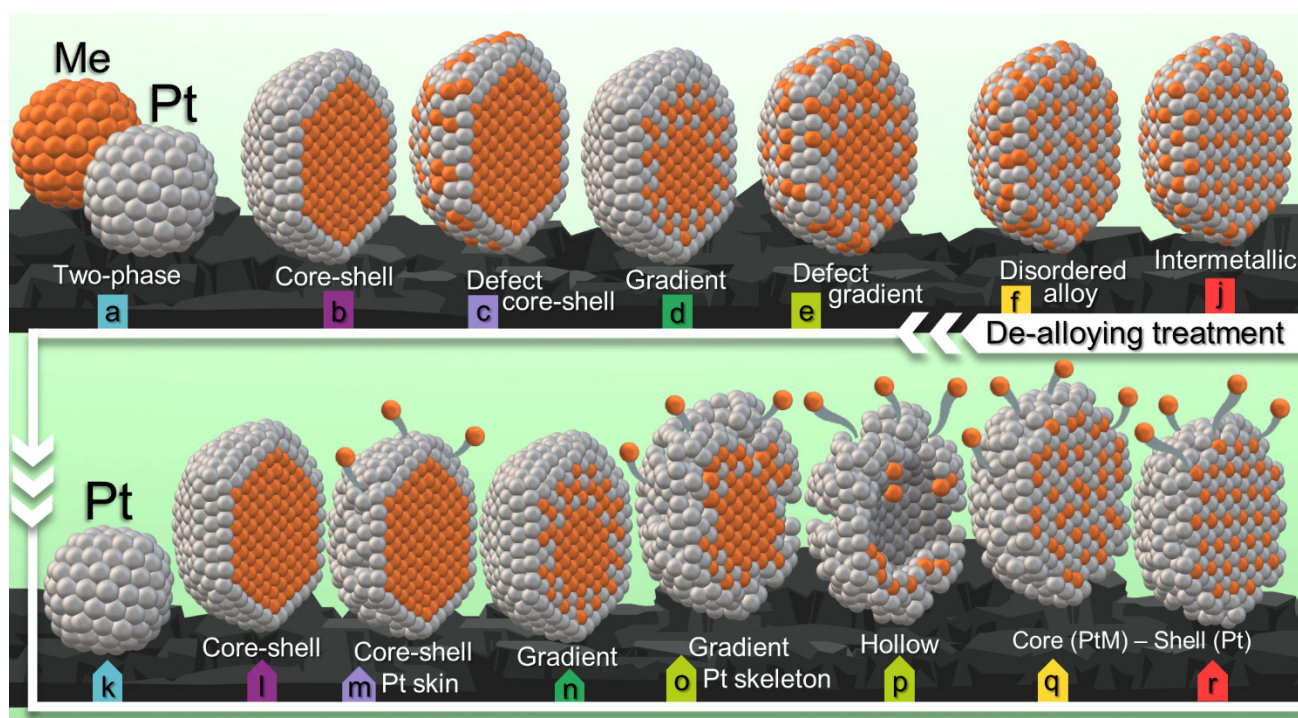


Figure 2. Scheme of possible transitions of bimetallic NPs structures under the influence of de-alloyed pre-treatment: (a) two-phase, (b,l) core-shell, (c) defect core-shell, (d,n) gradient, (e) defect gradient, (f) disorder alloy, (j) intermetallic, (k) Pt phase, (m) core-shell Pt skin, (o) gradient Pt skeleton, (p) hollow, (q,r) core(PtM)-shell(Pt) with order PtM alloy (r) or disorder PtM alloy (q). Platinum atoms are marked in gray; atoms of the alloying component are marked in orange. The top row represents examples of bimetallic nanoparticles structures in the “as-prepared” state. The bottom row represents the bimetallic particles structures after de-alloying treatment. The process of atoms of the alloying component dissolution is shown. The background color of the letters corresponds to the same structure before and after processing.

In [39], the authors investigated the compositions of NPs of different sizes in one material. During the study, Gan et al. confirmed that the composition of the “as-prepared” and acid-treated NPs differed vital only for large NPs bigger than 13 nm. The influence of the atmosphere on the formation of NP porosity has been proven. When treated in an air atmosphere, oxygen binds to the platinum atoms, thereby slowing down its diffusion. Thus, it is leaving the pores open, which favorably affects the leaching of the alloying component. For large particles, it has been shown that treatment in an air atmosphere led to a thickening of the platinum shell, while this effect is absent in an oxygen-free atmosphere [39]. The article concludes that it is necessary to obtain materials based on small NPs (less than 10 nm). In this case, the NPs will be more homogeneous (even) in composition, will retain more of the alloying component (in the core) and will be more stable.

In [23], the authors obtained a CuPt_3 alloy by polyol microwave-assisted synthesis with co-reduction of precursors on a carbon support. To form a core-shell structure of NPs, the resulting catalyst is treated in nitric acid. The authors demonstrate the determination of the NPs surface composition by the X-ray photoelectron spectroscopy (XPS) method, which differs from the bulk composition (inductively coupled plasma (ICP) and energy-dispersive X-ray (EDX) analysis), that confirms the formation of the core-shell. In this study, the de-alloyed catalyst exhibits 1.8 and 3.3 times higher mass activity compared to the “as-prepared” material and commercial Pt/C samples (HiSPEC 4000, Johnson Matthey), respectively.

In [42,43], the authors synthesized PtNi/C and PtCo/C catalysts with NPs with a hollow structure. It is noted that the content of the alloying component after acid treatment

varies from 2 to 8 at. % for the presented materials, despite the d-metal high content in the initial state.

Hollow PtNi NPs with a core–shell structure were obtained by treatment in 0.01 M HCl [37]. It was noted that with an increase in the acid concentration by a factor of 10, nickel is completely leached out, leaving a hollow platinum NP. De-alloyed Pt-Ni is characterized by a higher mass activity in ORR compared to the as-prepared material, as well as hollow Pt and a commercial sample.

A systematic study of the acid treatment effect on the structural and functional characteristics of the PtCu/C catalyst is presented in [36]. The authors carried out acid treatment of the PtCu/C catalyst with various acids, HNO₃, H₂SO₄, and HClO₄. As a result of the study, a positive effect was found to increase the catalysts ORR activity when using 1 M HNO₃ to obtain de-alloyed PtCu/C. The authors attribute the effect of increased activity in the ORR to the high content of copper in the de-alloyed materials. Increasing the acid concentration to 5M leads to a decrease in the copper content and, consequently, to a decrease in the ORR activity. The works [36,44] demonstrate the possibility of successfully using catalysts in the MEA after treatment in 1 M HNO₃.

Previously, in [45], we showed that the acid treatment of materials based on NPs with a “gradient” structure can lead to a decrease in specific activity in the ORR.

Gatalo et al. [40] are among the few researchers to study the behavior of chemically prepared de-alloyed catalysts without electrochemical activation cycling. The initial Pt-Cu NPs were obtained by annealing a copper precursor with gelatin on a carbon support and subsequent galvanic substitution of Cu for Pt. To obtain a de-alloyed structure, the authors use a 4-fold acid wash to simulate the exchange in the electrolyte during electrochemical activation. The use of CO makes it possible to block the platinum surface and prevent copper deposition on it. The unique ex situ activation method of the PtCu/C catalyst presented in this work makes it possible to achieve the highest mass activity in the ORR reported in the literature.

The preparation of bimetallic catalysts is possible not only by reducing both precursors, but also by impregnating Pt/C catalysts with a d-metal salt, followed by reduction and fusion in a hydrogen atmosphere [35]. The authors of the work [35] demonstrated gradient strain effect in de-alloyed Pt-Fe NPs by computer processing on the real objects (particle size is 4–5 nm). The PtFe/C catalyst presented in this work is characterized by a 2-fold higher mass activity compared to the commercial analogue of Pt/C (HiSPEC 3000, Johnson Matthey).

Note that there are several studies using organic compounds in acid treatment, such as acetic acid [40] and dimethylglyoxime [38]. In contrast to the easy method for the synthesis of PtNi/C catalysts obtained by the co-reduction of precursors with sodium borohydride in [42], the authors of [38] prepare Pt-Ni NPs using expensive organometallic precursors (acetylacetonate) in an organic medium in the presence of stabilizing agents. However, [38] submitted a unique method of de-alloying. Octahedral NPs are dissolved in an aqueous solution of dimethylglyoxime, which selectively coordinates nickel from oxide, so the presence of oxygen has a vital impact. The authors performed an identical experiment in an oxygen-free atmosphere and did not obtain a de-alloying process. It has been shown that the alloy has a limiting composition, which is no longer amenable to de-alloying—Pt₃Ni. Articles have also demonstrated the process of forming a concave structure from octahedral NPs step by step. The authors show that the etching process involves the faces of {100}, {110}, and {111} particles in different sequences, resulting in a concave structure. As the initial nickel content increased, the NP concavity after etching increased too. The study also showed that a concave structure can be obtained from cubic NPs. Acid treatment with concentrated nitric acid was noted to lead to NPs aggregation and concave structure destruction [38].

2.2. Electrochemical Activation

The study of the electrochemical characteristics of catalysts for PEMFC always begins with the stage of electrochemical activation of PtM/C materials in an acidic electrolyte. During this stage, as well as during the subsequent operation of the catalysts, the composition and structure of NPs evolve, which determines the features of their electrochemical behavior [46–50]. It became clear that earlier researchers often obtained an electrocatalyst of a certain composition/structure, while the functional characteristics were studied for a catalyst with a changed composition and structure (architecture) of NPs [15,51].

Now, the stage of electrochemical activation is considered to be an obligatory stage of bimetallic catalysts de-alloying and is the initial stage of all electrochemical measurements of such materials (Table 2). An analysis of the publications shows that voltametric activation can be carried out in a different range of potentials [52–54], at different potential sweep rates (from 50 to 1000 mV/s) [32,46,52], with a different number of cycles from 50 to 500 [32,46,52,54,55]. Some authors indicate that cycling is carried out until the type of cyclic voltammetry (CV) ceases to change [56–58]. Most often, researchers use activation in the potential range of 0.06–1.2 V [46,59], but sometimes in a wider range, for example, from 0.05–1.35 V [60]. It should be noted that most authors recommend a comparison and detailed study of the de-alloyed PtM/C catalysts behavior after activation cycling. In view of the above, it is important to understand that the composition and microstructure of such materials differ from the initial “as prepared” state.

We have studied the structure of materials after chemical and electrochemical treatment (Figure 3). X-ray diffraction patterns of a PtCu₃/C sample with a structure of solid solution demonstrate a shift of the (111) maximum to the region of smaller 2 theta angles after pre-treatment, which indicate a decrease in the copper content in crystallites (Figure 3a). In this case, the average crystallite size increases from 1.9 to 2.6 and 3.7 nm during chemical and electrochemical treatment, respectively.

The results of the transmission electron microscopy (TEM) photographs analysis showed that for Pt-Cu NPs with a core-shell structure, after treatment in nitric acid, the average NPs size decreases from 6.2 to 3.2 nm (Figure 3b–d). During electrochemical activation of the alloy sample in the potential range of 0.04–1.2 V, there is no change in the average size of spherical NPs; however, a significant fraction of rod-shaped NPs appear, as noted in our works [61,62] (Figure 3e–g). Thus, after de-alloy treatment, significant changes are observed in the structure of bimetallic catalysts.

In [46], a stage of electrochemical de-alloying presented as a stage of synthesis electrocatalysts. At the first step, a material with a high copper content is obtained and is subsequently treated in an acidic medium in a given potential range to remove copper. The authors believe that the selective electrochemical dissolution of alloying metal is the key process in the formation of the active catalyst.

Gatalo et al. [51] showed that electrochemical de-alloying leads to a significant change in the surface structure and morphology of catalyst NPs. At the same time, it was shown in [52] that the use of electrochemical de-alloying makes it possible to obtain catalysts with stable composition that remains during further electrochemical measurements. As a rule, such studies are carried out for catalysts containing large NPs (at least 10 nm). At the same time, to obtain catalysts, researchers use complex laboratory synthesis methods using stabilizing agents and low product yields, which are not suitable for technological use [63,64].

In [15], the authors studied the dissolution of alloying d-metals and platinum during electrochemical activation of PtM/C (M = Cu, Co, Ni and Fe) catalysts up to different values of the limiting potential. It has been shown that all metals making up the NPs dissolve during measurements. The dependences of the Pt dissolution rate on the potential were studied, at which insignificant anodic and higher cathodic peaks of Pt dissolution are observed [65–67]. The authors indicate that the mechanism of Pt anodic dissolution is associated with the appearance of a rough surface structure due to the oxide place-exchange mechanism [67]. The cathodic dissolution of platinum occurs during the reduction of Pt-

oxide, which also changes the metal surface and causes its dissolution in defective areas of nanocrystals [68]. The authors of [15,65] note that, after the dissolution of platinum from the surface layer of NPs in the case of PtM/C materials, the dissolution of M-atoms again occurs. That is, during the dissolution of Pt, atoms of the alloying metal are exposed, and their subsequent oxidation occurs [65].

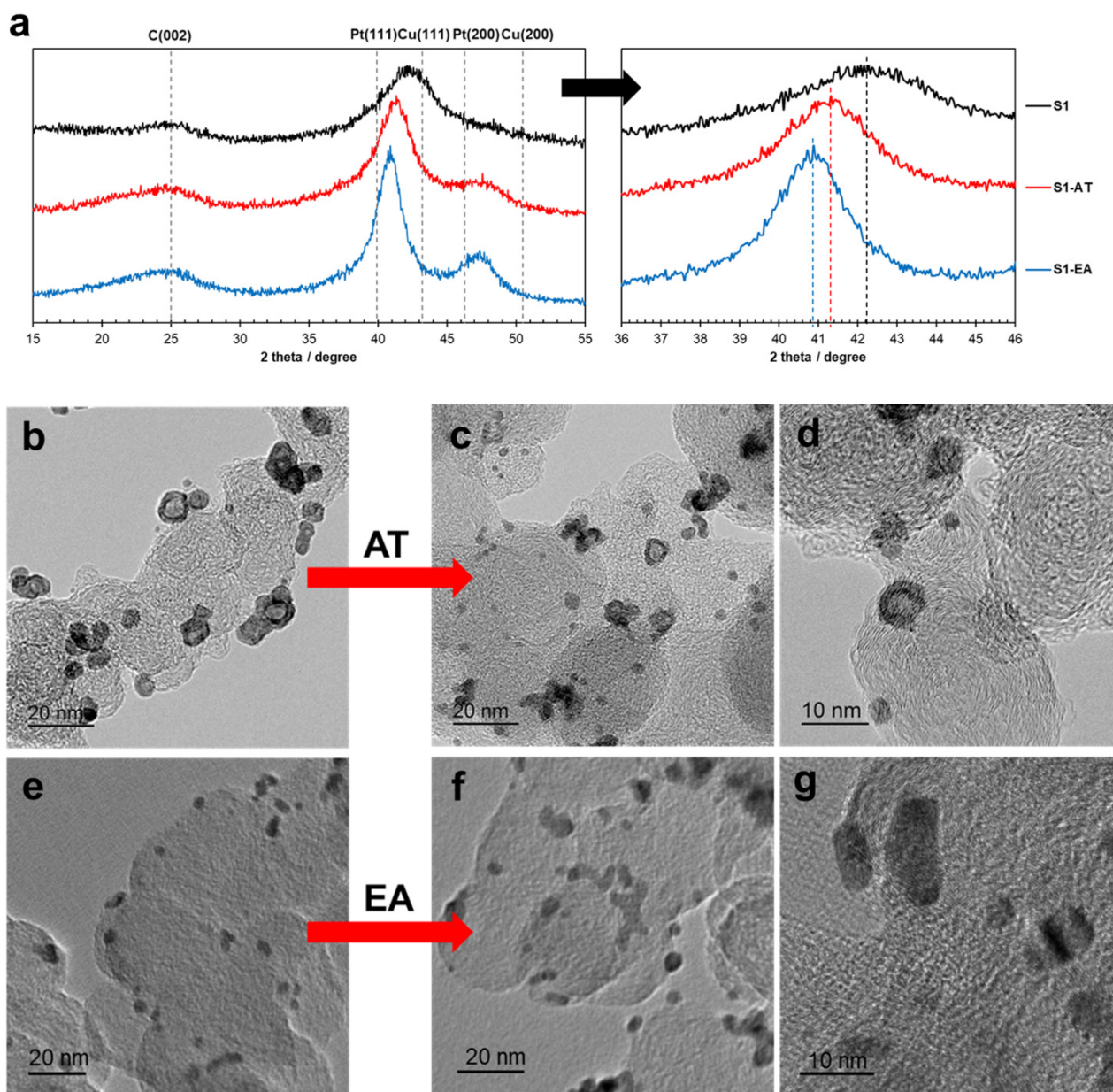


Figure 3. X-ray diffraction (XRD) patterns of PtCu/C materials with alloy structure of NPs (a): initial, after acid treatment and after electrochemical activation. TEM images of PtCu/C catalysts with core-shell (b–d) and alloy (e–g) structure: initial (b,e) and after acid (c,d) and electrochemical (f,g) de-alloying, respectively.

In [46], the authors describe a two-stage protocol of electrochemical de-alloying of bimetallic catalysts. At first, recordings of three CVs at a scan rate of 100 mV/s were performed, and then longer 200 cycles at scan rate of 1000 mVs⁻¹.

In [59], the authors present a protocol of electrochemical leaching in a three-stage process: (1) three slow scans with a scan rate of 100 mVs⁻¹, (2) 200 fast scans with 500 mVs⁻¹, and finally, (3) three slow scans with 100 mVs⁻¹.

The de-alloying of the catalysts was performed in two ways: (1) by sweeping the potential of the electrode from 0.05 to 1.2 V for 500 cycles at a scan rate of 0.2 Vs^{-1} and (2) by holding the potential at 1.2 V for 15 min or 2 h in a deaerated electrolyte [55].

As stated in a paper comparing two de-alloying protocols: the rapid dealloying of the catalysts at 1.2 V and the concomitant formation of highly porous structures for larger NPs leads to a certain accessibility of the inner part of the catalyst particles for the electrolyte. This can be attributed to the formation of stable Pt oxide at these high potentials and thus a reduced mobility of the surface Pt atoms, which are unable to passivate the surface and block Cu dissolution. In contrast, the potential variation during cycling induces not only Cu dissolution but also Pt oxide reduction accompanied by dissolution/redeposition and/or an increased surface mobility of Pt. As a consequence, this enables reordering of the Pt surface, giving rise to faceting, and prevents further dealloying. Porosity is thus observed only on larger particles in the case of extended potential cycling after 7000 degradation cycles.

In the course of electrochemical measurements, processes of not only de-alloying, but also re-alloying, associated with the redeposition of all components of nanoparticles, can occur, as well as during operation in an FC [69–71]. Such processes can occur even after the acid pre-treatment of bimetallic catalysts [70].

The authors of most publications devoted to a structural characteristics detailed study of de-alloyed catalysts obtained both in the process of electrochemical activation and by acid treatment note that the investigation of individual NPs is possible at a size of at least 8–10 nm. Oezaslan et al. note that, in the process of electrochemical activation, NPs smaller than 5 nm in size are characterized by the presence of a residual core-shell structure with a defective platinum shell. For NPs with a size of 10–20 nm, the formation of a structure with several cores of the alloying component and its uneven distribution in the NP is characteristic in the process of de-alloying. The platinum shell in such materials is rough. Thanks to the in situ study of individual large NPs (more than 30 nm) subject to electrochemical activation, it can be argued that a porous structure is formed due to the removal of the alloying component [59]. In [33], the authors describe the formation of a porous structure for particles larger than 8 nm.

Thus, according to reviewed publications, various types of de-alloyed treatment of PtM/C catalysts make it possible to optimize the bimetallic nanoparticles composition and structure, which leads to an increase in their catalytic activity in ORR or stability.

3. Thermal Treatment

In addition to various types of PtM/C catalyst de-alloyed pre-treatment, which are detailed in the previous section, heat treatment is used to improve the materials functional characteristic. It can have a positive effect on the properties of catalysts various types containing both platinum and bi- and trimetallic platinum-based NPs. The publications describe many studies aimed at optimizing the heat treatment process. Thus, in the review [29], the main mechanisms of the heat treatment effect on such catalyst properties as particle size, morphology, metal distribution on the support, alloying degree, formation of active sites, activity, and stability were considered. The optimum heat treatment temperature and time to increase the ORR activity and stability depend on the particular type of catalyst. In general, there are two effects caused by heat treatment: (1) change in the support surface functional groups and (2) change in the Pt distribution, morphology, and crystallite growth on the carbon support. Several models are also noted to explain the mechanisms of sintering and particle growth: (a) the migration and coalescence of particles and (b) Ostwald ripening. In the first mechanism, the movement of metal particles on the support surface occurs through the migration of Pt or PtM NPs. The second mechanism involves the exchange of atoms, with larger particles grow and smaller particles continuously decrease in size. This process is like the Ostwald ripening of dispersed precipitates in solution. In this case, the degree of NPs enlargement depends on the initial size and composition of NPs, the nature of their distribution in size and on the surface of the carbon support, and also the type of support. It is known that heat treatment can cause an increase

in particle size, a better degree of alloying and a change in the surface morphology of the catalyst from amorphous to a more ordered state, which has a noticeable effect on the activity and stability of the catalysts.

There are many parameters that can be varied during the heat treatment process, such as atmosphere, temperature, and duration. As a rule, heat treatment is carried out in an inert (N_2 , Ar or He) or reducing (H_2) atmosphere in the temperature range of 80–900 °C for 1–4 h [29], but in a few studies, 7 or more hours have been applied [72,73].

3.1. Pt/C Catalysts

Studying the effect of heat treatment on the structure and activity of materials is the simplest for Pt/C catalysts.

For Pt/C catalysts, thermal treatment leads to an increase in the size of platinum NPs [74–82] and to a wider size distribution of Pt particles [74,76,77,79,82], which, in some cases, leads to a significant decrease in the electrochemically active surface area (ESA) value [78,81–83] and in the catalysts mass activity [74,78,81,82,84]. On the other hand, heat treatment improves the crystallinity of Pt, which, in turn, leads to an increase in specific activity. The authors of [76] believe that during heat treatment, Pt particles are formed in a cubo-octahedron shape with well-defined faces. These opposite trends determine the existence of an optimal treatment temperature in terms of catalytic activity. That is why it is so important to determine the optimal temperature, atmosphere and duration of heat treatment. Thus, the authors of [76] think that heat treatment at a temperature of about 550 °C H_2/N_2 for 9 h improves the crystallinity of the Pt particles surface, which increases the catalytic activity. The authors of [74] indicate 600 °C 5% H_2/N_2 2 h as the optimal temperature for increasing the catalytic activity.

Thus, even for simple Pt/C systems, the optimal treatment temperature differs significantly for different researchers, which can be associated both with various treatment conditions, and with different structure of materials before treatment, particle size and size distribution, type of carbon support, the uniformity of the NPs distribution over the carbon support surface, the Pt NPs shape, etc.

3.2. PtM/C Catalysts

The study of the heat treatment effect on the structural and functional characteristics of bi- and trimetallic catalysts has also been developed. Given the complexity of such systems, many factors have been identified that affect the architecture, activity, and stability of such catalysts.

Many publications describe a linear correlation between the specific activity of Pt–M catalysts in the ORR and the average Pt–Pt interatomic distance in bimetallic NPs. The smaller the average interatomic distance Pt–Pt, the higher the activity of the catalyst in the ORR. Thermal treatment of the bimetallic catalyst at temperatures above 700 °C has two opposite effects: (1) the formation of a higher quality Pt–M alloy, which reduces the Pt–Pt distance, affects the d-band center and thus improves the specific activity of Pt and (2) an increase in the size of the bimetallic NPs, resulting in a reduction in the ESA, which leads to a decrease in the catalyst mass activity [29]. Many authors note the greater activity and stability of intermetallic compounds (ordered structure) compared to disordered solid solutions [73,85,86]. All these factors determine the presence of the optimal treatment temperature depending on the bimetallic NPs composition. It is important to note that when choosing heat treatment conditions, it is important to consider the architecture of bimetallic nanoparticles, such as core–shell (Figure 4a–d), gradient (Figure 4e–h), and hollow structure.

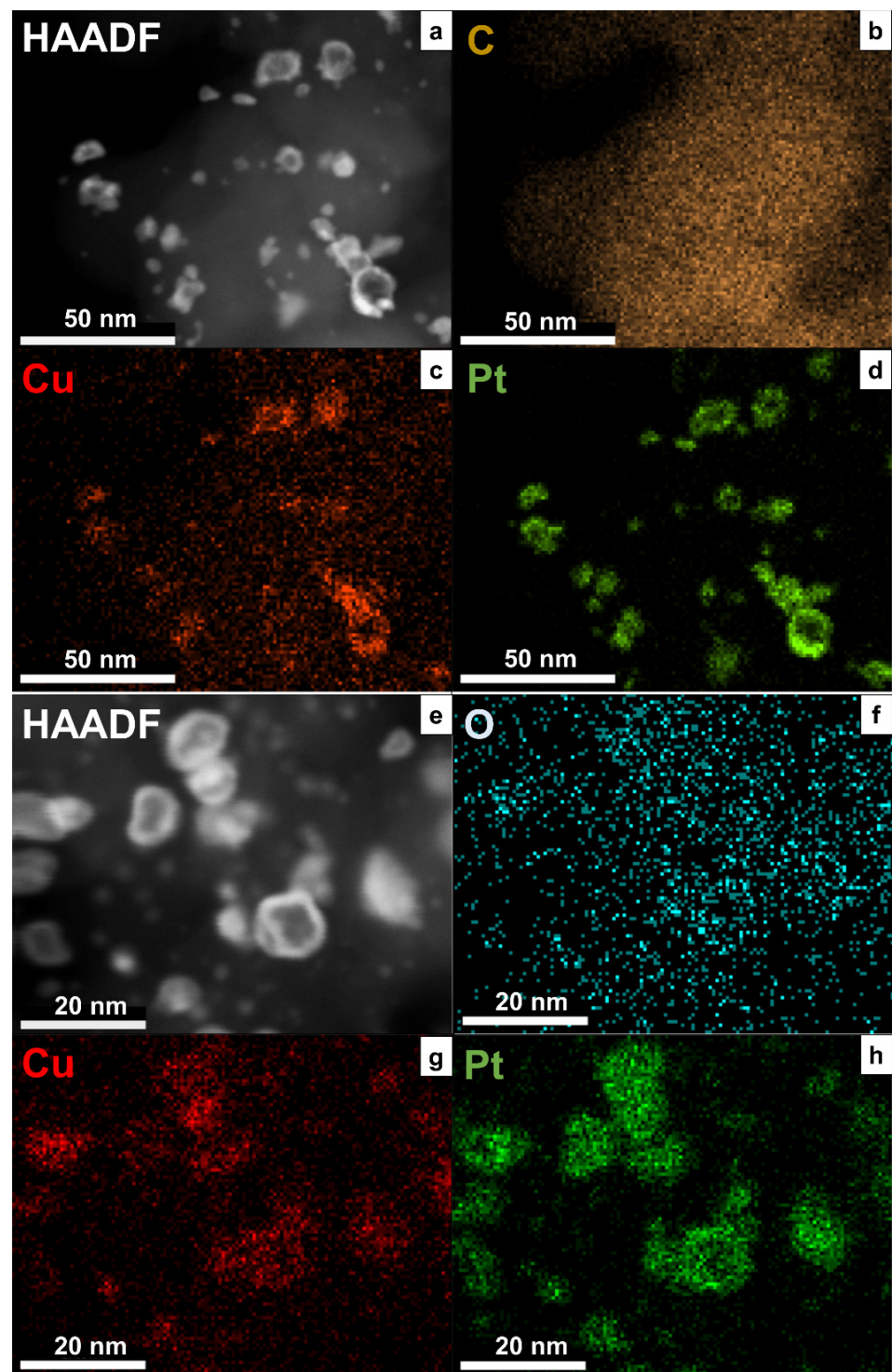


Figure 4. HAADF STEM for PtCu nanoparticles with core–shell structure (a) and with “gradient” structure (e) and EDX mapping of C (b), Cu (c,g), Pt (d,h), O (f) for these materials.

During heat treatment, the architecture of bimetallic NPs can be transformed (see Figure 5). For example, nanoparticles with a special architecture, such as core–shell (Figure 5b), gradient (Figure 5d), hollow (Figure 5j), or two separate nanoparticles of different composition (Figure 5f) when heated due to the mutual diffusion of atoms, under certain conditions, can transform into a disordered alloy (Figure 5l) or an ordered alloy (Figure 5k). On the other hand, when heated, in some cases, bimetallic nanoparticles with

an alloy structure (Figure 5a) can transform into core-shell structures due to the segregation of atoms of one of the metals on the nanoparticles surface (Figure 5m). Thus, the transformation of the core-shell structure into an alloy was shown at a temperature of about 280 °C for the PtCu NPs with a shell-core structure according to ex situ heating data [87–89]. In addition, when PtCu C materials are heated to temperatures above 300–350 °C, the formation of an ordered structure of PtCu NPs is observed [87,88].

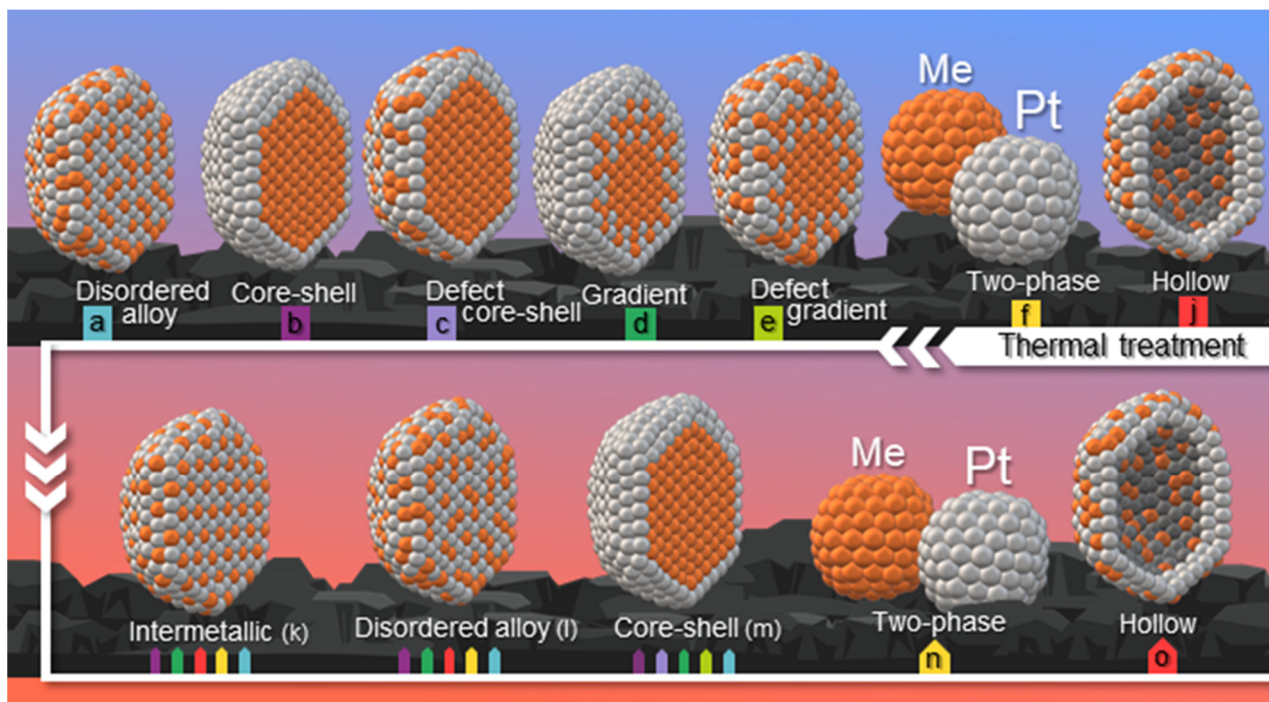


Figure 5. Scheme of possible transitions in the structures of bimetallic NPs under the heat treatment: (a,l) disorder alloy, (b,m) core-shell, (c) defect core-shell, (d) gradient, (e)defect gradient, (f,n) two-phase, (j,o) hollow, (k) intermetallic. Platinum atoms are marked in gray; atoms of the alloying component are marked in orange. The top row represents examples of bimetallic nanoparticles structures in the “as-prepared” state. The bottom row represents the bimetallic particles structures after heat treatment. The background color of the letters corresponds to the same structure before and after processing.

3.3. PtCo/C Catalysts

PtCo/C catalysts are widely used among bimetallic catalysts due to their high activity [90]. It is also known that Toyota uses such catalysts in the production of low-temperature fuel cells for Mirai car, which confirms the importance of commercializing such systems [91].

In [92], heat treatment was carried out in an atmosphere of 5% H₂/95% N₂ at a temperature of 50, 100, 200, 300, 400 and 500 °C for 2 h and cooled to room temperature. The authors point out that, according to the results of EDX, core-shell-type NPs are initially formed at a treatment temperature of 300 °C. The results of in situ X-ray diffraction show that heat treatment promotes the formation of a crystal structure and an optimal particle size distribution of 3–5 nm. The optimal temperature for heat treatment varies in the range of 300–400 °C (see Table 3) [92,93]. Table 3 summarizes some of the heat treatment conditions, structural characteristics and activity in the ORR for various Pt-based catalysts described in the publication.

Table 3. Structural and electrochemical characteristics of bimetallic catalysts after thermal pre-treatment.

Sample	Composition	Pt [wt.%]	Type of Support	Heat-Treatment Conditions			Particle Size, nm		Lattice Constant (Å)	ESA, m ² /g(Pt)	Activity, MA g ⁻¹ at 1600 rpm E = 0.9 V, Unless Otherwise Stated	Ref.
				Treatment Temperature T, °C	Atmosphere	Time Period t (h)	XRD	TEM				
Pt/C	Pt	20	Vulcan XC-72R		As-prepared		2.4	-	3.958	56.3	188 (0.75 V)	[80]
				900	H ₂ (5.2 mol.%)/Ar	1/12	3.3	-	3.928	31.7	125 (0.75 V)	
PtCo/C	Pt ₃₀ Co ₇₀	11.7	Vulcan XC-72R		As-prepared		1.2	-	3.920	17.5	186 (0.75 V)	
				900	H ₂ (5.2 mol.%)/Ar	1/12	25.5	-	3.720	30	84 (0.75 V)	
PtCr/C	Pt ₃₀ Cr ₇₀	12.3	Vulcan XC-72R		As-prepared		2.7	-	3.923	26.2	158 (0.75 V)	
				900	H ₂ (5.2 mol.%)/Ar	1/12	12.8	-	3.868	16.1	140 (0.75 V)	
PtCoCr/C	Pt ₃₀ Co ₃₀ Cr ₄₀	12.1	Vulcan XC-72R		As-prepared		2.2	-	3.914	17.0	152 (0.75 V)	
				900	H ₂ (5.2 mol.%)/Ar	1/12	7.3	-	3.774	6.27	111 (0.75 V)	
PtCo/C	PtCo ₃	22	HSAC *	650	4 vol.% H ₂ / 96 vol.% Ar, flux 100 mL min ⁻¹ ,	7	1.8	-	3.749	40 ± 4	280 ± 50	
				800			2.2	-	3.726	45 ± 4	380 ± 50	
				900			3.2	-	3.717	37 ± 2	290 ± 40	
PtCu/C	PtCu ₃	22	HSAC *	800			3.6	-	3.705	47 ± 2	410 ± 90	
PtCo/C	Pt ₃ Co	18.2	Vulcan XC-72		As-prepared		2.7	3.0	3.924	49	-	
				300			3.4	3.2	3.911	41	-	
				400	H ₂ (10%)/N ₂ (90%)	2	3.8	3.5	3.912	66	-	
				500			4.3	3.6	3.912	54	-	
				600			5.8	4.1	3.913	30	-	
PtCo@Pt/C	PtCo	60	Vulcan XC-72	360	H ₂ /N ₂	3	5.0	-	3.827	31.1	52.9	
				500	H ₂ /N ₂	16	5.4	-	3.803	28.4	53.6	
Pt ₃ Co/C	Pt ₃ Co	**	Vulcan XC-72	400	H ₂	2	4.8 ± 1	-	3.873	51.6 ***	160	
				700			7.2 ± 1	-	3.841	47.3 ***	520	

Table 3. Cont.

Sample	Composition	Pt [wt.%]	Type of Support	Heat-Treatment Conditions			Particle Size, nm		Lattice Constant (Å)	ESA, m ² /g(Pt)	Activity, MA g ⁻¹ at 1600 rpm E = 0.9 V, Unless Otherwise Stated	Ref.
				Treatment Temperature T, °C	Atmosphere	Time Period t (h)	XRD	TEM				
Co@Pt/C	Pt ₃ Co	36.3	Vulcan XC-72		As-prepared		2.7	2.4	-	-	21.2	[92]
				300	H ₂ /N ₂ (5%/95%), 40 mL s ⁻¹	2	3.8	3.0	-	-	50.3	
Pt ₃ Co/C	Pt ₃ Co	-	Vulcan XC-72		As-prepared		2.2	2.5 ± 0.3	2.24	44	136	[83]
				200	H ₂ /Ar		3.2	3.0 ± 0.5	2.24	52	129	
				500			4.1	3.9 ± 1.2	2.24	36	217	
PtNi/C		6.79	Vulcan XC-72		As-prepared					31.3	13.3	[96]
				350	H ₂ /N ₂ (20%/80%)	6	-	-	-	18.7	267.6	
				700	H ₂ /N ₂ (20%/80%)	2	-	-	-	21.6	27.5	
PtNi/C	Pt ₃₄ Ni ₆₆	15	Vulcan XC-72R		As-prepared		-	8.4 ± 1.1	3.771	33	1700	[97]
				300	H ₂ /N _{2,45} (4%/96%)	1	-	8.3 ± 1.2	3.777	32	2700	
				500			-	9.4 ± 1.2	3.755	43	700	
PtCu/C	Pt _{0.8} Cu	21.3	Vulcan XC-72		As-prepared			4.8	3.843	55 ± 5	132	[87]
				250	Ar	1	-	-	3.847	58 ± 6	116	
				280			-	5.8	3.829	56 ± 6	151	
				300			-	5.9	3.798	41 ± 4	225	
				350			-	-	3.777	31 ± 3	43	
400	-	-	3.873	83.2			49.1					
PtCu/C	Pt ₂₀ Cu ₈₀	11	O-CNTS ****		As-prepared							[98]
				500	H ₂ (5%)/Ar	6	4.3	2.7	3.882	68.9	60.8	
				600			4.6	3.7	3.837	50.0	39.4	

* High surface area carbon; ** In a typical synthesis, 53.3 mg of H₂PtCl₆ · 6H₂O and 8.2 mg of CoCl₂ · 6H₂O were. *** Values are calculated based on the results presented in the article dissolved in deionized water, and 78 mg of Vulcan XC-72; **** Oxygen functionalized carbon nanotubes.

In [99], heat treatment was carried out in an atmosphere of 5% H₂/N₂ at 500 °C for 1 h after pre-treatment in 0.5 M H₂SO₄. The catalysts were synthesized using a polyol reduction method (Pt deposition) followed by the impregnation method (joint mixing of precursors for 24 h, then heating at 900 °C for 1 h). The pre-leaching process reduces the percentage of metallic Pt on the catalyst surface due to its oxidation by various forms of oxygen. However, metallic Pt can be restored to its initial conditions by heat treatment. In addition, the study claims that the maximum catalyst specific power loss of the heat-treated catalyst after leaching is 9%, while the unheated catalyst loses 28% of the initial maximum specific power, indicating a heat-treated catalyst with greater stability. The authors attribute this to a smaller increase in particle size after treatment and a better distribution of particles over the carbon support.

Heat treatment of Pt-Co catalyst was carried out for 16 h at 500, 550, 600, and 700 °C in an H₂/N₂ atmosphere [73]. Intermetallic PtCo@Pt core-shell NPs on a carbon support with a metal content of up to 60% have been synthesized. The results of XRD and high-resolution TEM clearly show that after heat treatment, the face centered cubic (FCC) structure of the catalyst was transformed into an ordered face centered tetragonal (FCT) structure (see Figure 2) [99]. The ordered NPs show improved ORR performance compared to disordered PtCo/C catalysts and commercial Pt/C catalysts (see Table 3). An increase in the ORR activity of the ordered PtCo@Pt/C catalyst is presumably associated with a small particle size, a platinum-rich shell, lattice contraction, and enhanced d-hybridization [95]. The increased stability can be mainly associated with the ordered structure of the catalyst. Therefore, it is assumed that, as a result of the mutual diffusion of atoms, a shell of Pt atoms is formed on the ordered surface of intermetallic particles, which will enhance the ORR [83,100]. The authors suggest the optimal temperature is 550 °C, because at this temperature, the formation of an ordered structure occurs with the smallest enlargement of NPs. Additionally, ordered PtCo@Pt/C exhibits SA in the ORR five times higher than commercial Pt/C (60%, Johnson Mattew).

In [101], the heat treatment of Pt₃Co/C catalysts preparations by the impregnation reduction method was carried out at 700, 800, and 900 °C in an atmosphere of 8% H₂/Ar for 5 h. The temperature of 700 °C was characterized by the smallest particle size, but also the lowest degree of alloying. Despite the relatively high ESA for Pt₃Co-700, the catalyst exhibits low activity. As the temperature rises to 900 °C, the degree of alloying increases to the composition Pt₃Co. On the other hand, heat treatment leads to significant agglomeration of the NPs, resulting in a decrease in ESA and low mass activity. Nanoparticles synthesized at 800 °C achieve a sustainable balance between particle size and alloying degree, which ensures the highest mass activity and high enough stability. Therefore, 800 °C is the optimal temperature for the synthesis of Pt₃Co/C. The authors of [94] also consider the temperature of 800 °C for 7 h in a reducing atmosphere to be 4 vol. % H₂/96 vol. % Ar, at which the maximum value of ESA is reached, and the activity in the ORR increases relative to other samples and commercial Pt/HSAC (see Table 3). Additionally, in [80], a higher specific activity of PtCo/C is shown when treated at a high temperature of 900 °C.

In [102], the thermal stability of Pt₃Co NPs was studied by the molecular dynamics method. There are two types of structures: a chemically disordered alloy and an ordered intermetallic compound were studied. In addition, model NPs with a shell-core structure were studied, where the core was Pt₃Co coated with a shell of platinum or cobalt two atomic layers. The results of computer simulation show that ordered Pt₃Co intermetallic NPs demonstrate better thermal stability than disordered alloy particles. In the case of NPs with a core-shell structure, NPs with a Pt-shell are significantly superior in thermal stability to NPs with a Co-shell.

Thus, the optimum treating temperature and atmosphere directly depends on the initial structure of the resulting PtCo/C catalyst. Most researchers are of the opinion that higher treatment temperatures for PtCo/C catalysts ($\geq 700^\circ\text{C}$) in a reducing atmosphere are necessary.

3.4. PtNi/C Catalysts

PtNi-containing catalysts on a nanotube support were studied in [103]. Heat-treatment conditions were N₂, 30 min, 200 and 400 °C. The catalysts were synthesized by the polyol method using ethylene glycol as a solvent and reducing agent. The authors note that, according to XRD results, with an increase in the heat treatment temperature, the Pt {111} peak for PtNi/FCNTs catalysts shifts towards smaller 2θ angles compared to the “as prepared” sample, especially for catalysts treated at a temperature of 400 °C. This is explained by the phase separation between Pt and Ni because of the formation of nickel oxides during the heat treatment. Thus, in this case, there is no additional alloying of metals and a decrease in the interatomic distance. Except for PtNi (1:1), all bimetallic samples show almost no features of hydrogen adsorption/desorption in the second CV (after oxidation of the CO monolayer). However, after heat treatment, the peaks appear much stronger, which indicates the formation of the surface enriched in platinum. In addition, for almost all PtNi/FCNT electrocatalysts, despite an increase in the size of NPs, ESA increases after heat treatment, as in [104]. Since only surface Pt is detected during ESA measurements and no Ni, these results confirm the assumption of a more Pt-rich surface after heat treatment at 400 °C [105]. XPS indicated a very high Pt:Ni ratio; however, these values decreased after heat treatment. The nickel-depleted surface with structural changes and its segregation after heat treatment corresponds to this model. In this way, the authors prove a PtNi alloy core surrounded by a platinum-enriched shell with some nickel oxides present on the outside. Heat treatment at 400 °C in an N₂ atmosphere also led to phase separation/restructuring of the catalysts [106]. Heat treatment at 200 °C increases the mass activity for most PtNi/FCNT catalysts, but at 400 °C, it sharply decreases compared to the “as prepared” catalyst. However, materials treated at 400 °C are more stable after 200 cycles in the range of 0.2–1 V vs. Ag/AgCl. As noted in [96,97], if it is necessary to maintain a certain shape of the particles, the heat treatment should be performed very carefully. In [107], the authors indicate that stepwise heating to 800 °C in an air atmosphere transforms the precursor into a disordered nanoalloy PtNi. Then, upon subsequent slow cooling to 400 °C, a partially ordered structure is obtained. A disordered nanoalloy takes time to restructure. The atoms slowly migrate from their random positions to their energy-preferred positions in the unit cell, forming an ordered alloy structure. The authors note the importance of the cooling rate. Thus, to achieve complete ordering, it is necessary to cool the alloy to room temperature relatively slowly. With rapid cooling, only a disordered structure is obtained. Thus, not only do the heating rate and holding time during heat treatment affect the structure of the obtained materials, but so do the conditions for cooling the samples after treatment.

The authors of [106] describe the influence of the heat treatment atmosphere (vacuum, air, Ar, N₂, and H₂) and the treatment temperatures (250, 300, 350, 400 °C for 30 min). It has been established that the ESA does not change during treatment in a vacuum; it changes little in air, but the width of the double-layer region increases. In Ar, it sharply decreases at temperatures above 300 °C, and the shape of the CV changes too. These data are confirmed by the determination of the ESA by CO-stripping. The catalytic activity in a vacuum gradually decreases; when treated in air, it decreases by 2 times at a temperature of 350 °C (more than in a vacuum). The activity during treatment in an Ar atmosphere decreases significantly following the ESA, especially at a temperature of 400 °C (a sharp drop in activity at ≥350 °C). The heat treatment of the catalyst in argon caused a clear nickel segregation on the surface along with the formation of a thin carbon layer at ≥350 °C, which covers the catalyst surface, resulting in a decrease in ESA and activity. The formation of an amorphous carbon layer on metal NPs was proved by subsequent treatment at 280 °C, which led to an increase in ESA.

Catalysts with a trimetallic NPs structure and the effect on its heat treatment are also of particular interest. For example, in [108], the heat treatment of Pd@Pt–Ni-containing catalysts was carried out in an H₂ atmosphere for 3 h at 80–300 °C. When treated at temperatures from 80 °C to 250 °C, the Pd core was covered with a Pt–Ni shell layer, and all

feature reflections on XRD were between the reflections of Pt and Ni. As the temperature increases, the degree of crystallinity improves, and the diffraction peaks do not shift. When the temperature rises to 300 °C, a peak of reduced nickel from oxide appears. This indicates Ni segregation, which means the incomplete insertion of Ni atoms into the Pt lattice and the incomplete formation of the alloy. With an increase from 80 °C to 200 °C, the size of the catalyst particles remained almost unchanged. At temperatures above 200 °C, the number of atoms (Pt+Ni) on the NPs surface is much greater than that of Pd. This shows that a suitable treatment temperature can provide energy for atomic migration, making Pt-Ni a more uniform coating on the Pd core surface. This contributes to the formation of a core-shell structure consisting of Pd as the core and Pt+Ni as the shell. A temperature of 300 °C is unsuitable for the heat treatment of Pd@Pt-Ni/C, while treatment at 200 °C has the highest mass ($0.39 \text{ A} \cdot \text{mg}^{-1} \text{ Pt}$) and specific activity ($0.69 \text{ mA} \cdot \text{cm}^{-2} \text{ Pt}$).

Thus, heat treatment of Ni-containing catalysts should be carried out with caution at temperatures > 300 °C due to the segregation of Ni, its oxides and Pt at these temperatures. In addition, as noted above, in the case of PtNi-containing catalysts, the composition of the atmosphere during treatment plays a very important role.

3.5. PtCu/C Catalysts

Heat treatment at various temperatures (N_2 , 500, 700, 875 °C, 1 h) of PtCu₃ materials obtained by various synthesis methods was carried and led to changes in the crystal structure of Pt-Cu alloys [86]. Based on the chemical composition ($\text{Pt}_{0.25}\text{Cu}_{0.75}$) and the phase diagram of Pt-Cu systems, there is a high probability that ordered PtCu₃ or PtCu phases are formed during the heat treatment [72,98]. With an increase in the heat treatment temperature, an alloying process took place, leading to the formation of an ordered PtCu₃ phase. In the case of the Pt-Cu/C-IMP sample (impregnation synthesis method), this process started at 500 °C and ended at 700 °C. The main structure of the Pt-Cu/C-IMP sample after heat treatment at 700 °C and 875 °C is intermetallic PtCu₃. An increase in the treatment temperature of the Pt-Cu/C-SC (impregnation in the presence of sodium citrate additive) samples led to different patterns. New peaks were observed at $\sim 20.5^\circ$ and $\sim 39.1^\circ$ after treatment at 500 °C, which indicates the formation of an ordered trigonal crystal structure of PtCu at this temperature. There are also reflections related to the PtCu₃ phase. The analysis of XRD shows that, in each group of Pt-Cu samples after treatment at a temperature of 700 °C, a well-ordered structure crystal structure was formed [109,110]. The ordered PtCu₃ structure was formed in the Pt-Cu/C-IMP samples, while the mixed ordered PtCu and PtCu₃ phases were formed in the Pt-Cu/C-POL (microwave-assisted polyol method) and Pt-Cu/C-SC samples. The highest activity was measured for Pt-Cu/C-POL samples treated at 700 °C for 1 h.

The authors of [111] perform heat treatments at higher temperatures than previously described—800 °C, 900 °C and 1000 °C for 10 h in an atmosphere of N_2/H_2 (9:1 in volume). Typical diffraction peaks in heat treated samples are clearly identified as an intermetallic phase PtCu₃ due to the transition of oxidized Cu to metallic. At the same time, the atomic fraction of Pt on the surface gradually increases with an increase in the heating temperature. The best performance is shown by PtCu₃/C-1000: the methanol oxidation reaction (MOR) activity of the catalysts is 4.6 times higher than that of the commercial Pt/C catalyst. The authors explain the high activity of PtCu₃/C-1000 by a decrease in the Pt-M bond length [112]. Moreover, PtCu₃/C-1000 also shows better stability, explained by the Pt-enriched surface, which can effectively prevent Cu dissolution.

The effect of heat treatment PtCu/C catalysts at temperatures of 250, 280, 300, 350 °C (1 h, Ar) was studied in [87]. The catalysts were prepared by the borohydride synthesis method. According to the EXAFS spectroscopy data of materials, heat treatment at 250 °C leads to the destruction of the core/shell interface [113], and heating of the same duration at higher temperatures leads to a less or more pronounced destruction of this architecture (the formation of a solid solution), the aggregation of NPs, and ordering of the alloy structure (formation of intermetallic). Heat treatment is accompanied by partial carbothermal

reduction of CuO inclusions to copper atoms, which are part of the NP. At the same time, after treating the material in the temperature range of 280–300 °C, platinum atoms still preferentially segregate in the surface layer. An example of the rearrangement of an individual PtCu bimetallic particle under the influence of an electron beam in a microscope is shown in Figure 6. This determines the optimal nature of the development of the NPs surface during the electrochemical activation of PtCu_280 and PtCu_300 samples, its enrichment with platinum, and relatively high catalytic activity. These samples are also characterized by minimal selective dissolution of copper. Increasing the treatment temperature to 350 °C leads to aggregation and increasing the NPs size, to increasing in the surface concentration and the rate of selective anodic dissolution of copper, to decreasing the ESA and mass activity in the ORR. Thus, from the point of view of the catalysts' maximum activity, the optimum temperature was about 280 °C. Additionally, in [84], the PtCu/C catalyst treated at 350 °C shows a 1.3-times increase the ORR activity compared to the "as-prepared" sample. This temperature is optimal, since already at 450 °C, the ORR activity of the catalyst has declined.

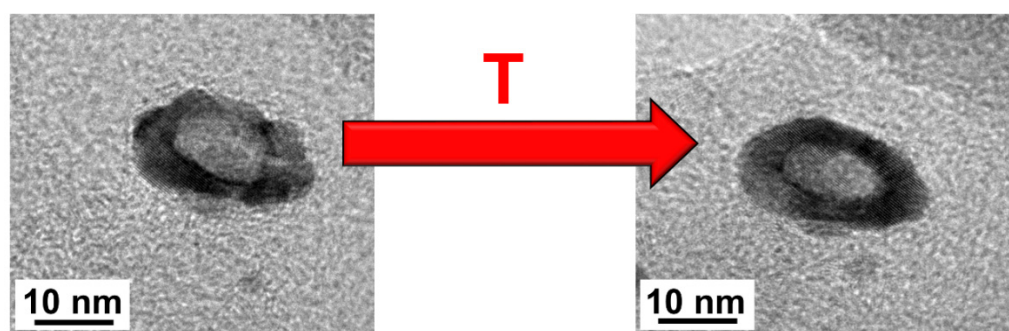


Figure 6. TEM images of PtCu nanoparticle with core–shell structure before and after heating by electron beam.

The growth of NPs at 500 and 800 °C (Ar and vacuum) was shown in situ [114]. The PtCu₃/C catalyst was prepared by a double passivation galvanic displacement method. The authors note that NPs do not change their position up to 500 °C but become more spherical [105]. The size of Pt–Cu NPs also slightly increases, while large acicular CuO NPs decrease in size, presumably due to the copper enrichment of Pt–Cu NPs. When the temperature was raised to 800 °C, the size of the NPs increased further, the particles changed their position, and the shapes became more irregular. After heating from 500 °C to 800 °C, the authors conclude that, in this particular case, the dominant mechanism of NP growth is fusion rather than Ostwald ripening, since the NPs physically move and then sinter. The authors note that when heated in situ to 800 °C, a significant drop in the copper content was observed. This conclusion is in sharp contrast to ex situ observations, indicating further Cu enrichment upon heating to 800 °C. The authors suggest that, in the present experiment, the rapid and almost complete loss of Cu at 800 °C is a consequence of the microscope operation in a low pressure (high vacuum) medium (1×10^{-5} Pa). It can be seen from the phase diagram (stability of Cu, Cu₂O and CuO as a function of temperature and oxygen partial pressure) that only the Cu phase is stable in a vacuum at 800 °C. The authors point out that the migration of Cu is due to diffusion (the system needs to achieve the chemical composition equilibrium). At the same time, the process of individual atoms' incorporation into the Pt–Cu crystal lattice is presumably due to both the lower enthalpy and the lower surface energy of the NPs compared to individual atoms. Cu enrichment in the case of ex situ observation is also responsible for the initial growth of Pt–Cu NPs at moderate temperatures (up to 500 °C); when heated to 800 °C, growth occurs mainly due to coalescence. However, the authors do not evaluate the electrochemical activity of catalysts, which is an important factor in studying the effect of heat treatment.

The effect of heat treatment on the structure and activity of trimetallic Cu-containing catalysts is also of interest for research. Thus, the effect of heat treatment in an inert atmosphere at 300 °C on the structure and activity in the methanol oxidation reaction of the obtained PtCuAu/C materials was studied in [89]. A decrease in the active surface area and activity in the methanol oxidation reaction after heat treatment was shown.

Thereby, in the case of PtCu/C catalysts, the ordering of the NPs is also important. There are different variants of intermetallic compounds formed as a result of heat treatment; therefore, for copper, the initial composition of NPs is important. Additionally, for PtCu-containing catalysts, a wide range of optimal temperatures is set—from 280 to 1000 °C.

3.6. PtCr/C Catalysts

Among the alloying components, Cr is used much less frequently than Cu, Ni, and Co, but there are a few publications that have presented the greater stability of PtCr/C materials [115–117]. Therefore, despite the relatively small number of works on the heat treatment of PtCr/C, these materials will also be considered in the review.

The heat treatment of the Pt₃Cr/C catalyst in H₂ (reductive) and N₂ (inert) atmospheres at 900 °C for 2 h was performed in [118]. The Pt₃Cr/C catalyst was synthesized by the borohydride synthesis method. After heat treatment in an H₂ atmosphere, according to XRD data, an additional Cr₂O₃ phase is formed, while this oxide is not formed during treatment in an N₂ atmosphere. Additionally, according to the results of XRD, heat treatment in both atmosphere causes particle sintering but promotes the alloying of the second metal into the Pt structure. The ORR activity of the heat-treated catalysts increased by 1.2 times in comparison with the untreated catalysts. However, the Pt₃Cr/C(H₂) catalyst exhibits low stability compared to other Pt₃Cr/C catalysts, which is probably due to the presence of Cr₂O₃ in the structure. Thus, the authors consider treatment under N₂ atmosphere at 900 °C to be the optimal conditions for the treatment of this catalyst type.

In [119], the heat treatment of the PtCr/C catalyst was carried out in the range of 500, 700, and 900 °C in an N₂ atmosphere for 2 h. The PtCr/C catalyst was prepared by the seeding/impregnation method using NaBH₄. According to XRD results, the peaks of the Pt with FCC structure shift towards large 2θ angles as the temperature increases, which indicates the fusion of metal components. An increase in the NPs size due to agglomeration is also observed, which led to a decrease in the ESA for all heat-treated catalysts except for PtCr/C-500. The ESA value of PtCr/C-500 increased by a factor of 1.15, which the authors attribute to the elimination of the catalyst amorphous structure; the activity value increased compared to the non-treated material. Additionally, the PtCr/C-500 catalyst is more stable than other PtCr/C samples presented in the paper. The PtCr/C-900 catalyst exhibits a higher ORR activity compared to other heat-treated catalysts, presumably due to the high degree of alloying. However, it has poor stability (1.31 times lower than PtCr/C-500) in acid medium after 1000 cycles. Therefore, the authors consider a temperature of 500 °C to be optimal.

The heat treatment of PtCr/C catalysts in an atmosphere of 10% H₂/90% N₂ at 700, 900, and 1100 °C for 2.5 h was carried out in [120]. With an increase in the treatment temperature, the degree of the metal components alloying increased too, and as a result of the stability test, the amount of dissolved Cr ions decreased. The catalysts after heat treatment at 900 °C showed the highest mass activity (an increase by 2.9–3.3 times compared to the initial values), as well as higher stability compared to other materials.

3.7. Comparison of Catalysts Heat Treatment Alloying with Various D-Metals

When comparing the effect of catalysts heat treatment alloying with various d-metals, it should be noted that the various methods for preparing catalysts and various approaches to assessing their structure and activity are used in publications. Therefore, in our opinion, the most effective way to compare the influence of alloying components is to analyze publications where the effect of heat treatment on the structure and functional properties of PtM/C (where M=Cu, Co, Cr, Ni, Fe, Pd, Au) catalysts is studied in one work.

The authors of [80] note the high specific activity of PtCo- and PtCr-containing catalysts after heat treatment for 5 min at 900 °C in an H₂/Ar flow (5.2 mol.% H₂). The catalysts were synthesized by the borohydride synthesis method. The relative order of specific activity in the ORR of heat-treated catalysts was PtCo/C-900 > PtCoCr/C-900 > PtCr/C-900 > Pt/C-900 > Pt/C, while mass activities were Pt/C > PtCr/C-900 > Pt/C-900 > PtCoCr/C-900 > PtCo/C-900 (see Table 3). This trend can be explained by the ESA values, which showed that a Pt-Cr alloy resulted in a Pt-rich catalyst surface than a Pt-Co alloy. The authors point out that, in the PtCoCr/C-900 catalyst, intermediate properties (ESA, mass and specific activity in the ORR) are established between the PtCo/C-900 and PtCr/C-900 catalysts, which suggests the electrochemical properties of the PtCoCr/C-900 catalysts can be controlled by varying the amounts of Co and Cr.

The effect of heat treatment in the temperature ranges from 650 °C to 900 °C for 7 h in a reducing atmosphere containing 4 vol. % H₂/96 vol. % Ar was investigated in [94]. The de-alloyed PtCo₃ electrocatalyst (800 °C/7 h) shows 3 times higher mass activity and 4–5 times higher specific activity in calculation than 28.2 wt.% Pt/C. The de-alloyed Pt-Co catalysts (800 °C/7 h) demonstrate the most favorable balance between mass and specific activity. The research results indicate that an increase in the treatment temperature causes an increase in the particle size at a given heat treatment time but does not cause additional incorporation of Co into the alloy and, consequently, a decrease in the lattice parameter of the alloy [121]. In the case of Pt and Cu, it shifted towards higher 2θ angles compared to the angles of pure Pt, which indicated a decrease in the lattice parameter and the formation of a copper-rich Pt-alloy, as in [84], where the activity in the ORR is placed in the following order: Pt-Cu/C (350 °C) > Pt-Fe/C (350 °C) > Pt-Ni/C (350 °C) > Pt-Co/C (250 °C) > Pt/C (350 °C). Voltammetry dissolution of a less noble metal can also lead to an increase in surface roughness. An increase in the total surface area of the particles can also contribute to an increase in mass activity. Thus, the authors note the possibility of increasing the ORR activity caused by surface roughness.

In [81], two different heat treatment conditions were used: (1) to create a completely ordered structure, the NPs were subjected to heat treatment at 500 °C for 1 h in H₂/Ar atmosphere; (2) for the segregation of Pt atoms on their surface to further increase the ORR activity, heat treatment was carried out at 150 °C for 1 h in CO atmosphere (99.9%). After heat treatment at 500 °C H₂/Ar, the NPs strongly agglomerated, and their size increased significantly. In the case of PtAu/C-500, ESA decreased by a factor of 5; in the case of PtPd/C-500, by a factor of 1.6; the ORR activity also decreased by a factor of 9 and 1.6, respectively. Due to heat treatment at 150 °C in CO atmosphere, structural modifications occurred for PtAu/C NPs, leading to an increase in the fraction of Pt {111} and an increase in the atomic fraction of Pt on their surface. There is also an increase in ESA and ORR activity of the PtAu/C-CO catalyst by a factor of 1.3. In the case of the PtPd/C samples, the surface and bulk compositions were almost the same in all cases, which means that there was no change in the surface composition upon heat treatment. For PtPd/C NPs, heat treatment in CO atmosphere reduces the d-band center of Pt, which facilitates the mechanism of the MOR. The PtPd/C-CO sample exhibits an increased activity in the ORR (1.3 times higher than the initial one).

In [122], heat treatment was carried out in the range from 30 to 800 °C in an H₂ atmosphere. It has been established that, at 100 °C, PdCu nanoparticles are characterized by an FCC-structure. At temperatures of 200 °C and 400 °C, PdCu nanoparticles phase segregation into a mixture of FCC with a disordered structure and a BCC with ordered structure are seen. The catalyst after heat treatment at 100 °C exhibits the highest mass activity (4 times higher than that of the other studied catalysts and 8 times higher than commercial Pd/C). With an increase in the treatment temperature, the mass activity decreases significantly. On the contrary, the value of specific activity at temperatures above 400 °C increases. The authors indicate that the surface with the FCC structure (100) contributes to an easier breaking of the O–O bond due to structural effects, and it significantly increases the activity in ORR.

In [123], heat treatment was performed at 250, 300, and 350 °C for 1 h in Ar atmosphere. The catalysts were synthesized by wet synthesis using NaBH_4 as a reducing agent. In the case of heat treatment of Cu-containing catalysts, a significant enlargement of NPs (by a factor of 5–5.6) occurs; for PtCo- and PtNi- containing catalysts, by a factor of 2. In the case of $\text{Pt}_{1.0}\text{Co}/\text{C}$ and $\text{Pt}_{2.7}\text{Ni}/\text{C}$ catalysts, the mass activity in the ORR increased by a factor of 2–2.5 after heat treatment at 350 °C.

The heat treatment at 900 °C for 2 h in an N_2 atmosphere was carried out in [124]. The catalysts were prepared by the borohydride synthesis method. The degree of alloying was arranged in the order $\text{H-PtCo}/\text{C} > \text{H-PtCr}/\text{C} > \text{PtCo}/\text{C} > \text{PtCr}/\text{C} > \text{H-PtPd}/\text{C} > \text{PtPd}/\text{C}$. The $\text{H-PtCr}/\text{C}$ and $\text{H-PtCo}/\text{C}$ catalysts showed higher corrosion resistance than the PtCr/C and PtCo/C catalysts, while the $\text{H-PtPd}/\text{C}$ catalyst showed lower corrosion resistance than the PtPd/C catalyst. The authors attribute the low stability of the $\text{H-PtPd}/\text{C}$ catalyst to its well-ordered state. It was considered the $\text{H-PtCo}/\text{C}$ catalyst to be the most suitable catalyst for FC.

In [125], the heat treatment of a trimetallic Pt-Co-Ni/C system was carried out at 500, 600 and 700 °C for 2 h in a H_2 atmosphere. The authors point out that in the Pt-Co-Ni alloy, the ordered intermetallic phase PtCo rather than PtNi predominates, while the Co/Ni atomic ratio and treatment temperature are the key to increasing the proportion of the $\text{PtCo}_x\text{Ni}_{1-x}/\text{C}$ intermetallic phase. For $\text{PtCo}_x\text{Ni}_{1-x}/\text{C}$ catalysts, $\text{PtCo}_{0.5}\text{Ni}_{0.5}/\text{C}$ showed a significant increase in activity and stability in the electrooxidation of formic acid, which is explained by the optimal geometric and electronic structure, as well as the ordered structure. Meanwhile, $\text{PtCo}_{0.5}\text{Ni}_{0.5}/\text{C-700}$ is more active and stable than $\text{PtCo}_{0.5}\text{Ni}_{0.5}/\text{C-500}$ and $\text{PtCo}_{0.5}\text{Ni}_{0.5}/\text{C-600}$ due to the increased degree of ordering. In addition, ordered $\text{PtCo}_x\text{Ni}_{1-x}/\text{C}$ intermetallic catalysts show a notable improvement in stability compared to an ordered intermetallic PtCo/C electrocatalyst. This is explained by the presence of Ni in the ordered catalysts $\text{PtCo}_x\text{Ni}_{1-x}/\text{C}$ very likely prevents Co leaching in the acid solution to maintain the ordered structure.

Thus, catalysts heat-treated at temperatures of 600 °C and above, in which Co is the alloying component, are most widely used. However, there is a small number of works describing heat treatment at a lower temperature of PtCo-containing catalysts, which also showed high performance. However, as previously stated, the optimal conditions for PtNi/C catalysts are not optimal for PtCo/C catalysts. In this case, comparing them with each other has some inaccuracy. The choice of optimal heat treatment conditions directly depends on the nature of the alloying component.

4. Combination of Various Types of Pre-Treatment

In several publications, there are several treatment types for the obtained samples. A combination of acid treatment and subsequent heat treatment is often used, due to which nanoparticles with a core-shell structure with a thin platinum shell are formed [81,99,126,127]. It has been shown that the defective surface of NPs formed after acid treatment is ordered during heat treatment, resulting in a significant increase in catalytic activity [127]. For example, for PtNi/C catalyst acid treatment in acetic acid, after synthesis, a platinum-enriched surface on octahedral Pt-Ni NPs is formed [127]. During subsequent heat treatment at 300 °C, a Pt-enriched surface is first formed, and then, at high temperatures of 500 °C, the formation of a Ni-rich surface is observed. The sample after acid treatment followed by heat treatment at 300 °C showed a higher activity in the ORR (by a factor of 1.3) than the sample after acid treatment. The sample after acid treatment followed by heat treatment at 500 °C, which showed the least ORR activity, remained stable after 4000 cycles, that was probably due to a change in the octahedral shape to a more spherical one. Additionally, in [99], for PtCo/C catalysts, due to the combination of acid and heat treatment, the maximum power density increases by 30% compared to the untreated sample. The maximum power density loss of the acid+heat-treated catalyst is 9%, while the PtCo/CN catalyst loses 28% of initial maximum power density. Additionally, some sources describe a combination of heat treatment followed by acid [96,128], where acid treatment is used to remove residual

base metal atoms on the platinum shell. It is worth noting the importance of choosing the right processing conditions, since a high temperature can lead not to the improvement of the platinum shell, but to the formation of solid solution NPs and, due to the mutual diffusion of atoms, to a significant increase in the NPs size, and, consequently, to a decrease in the ESA.

In our opinion, a very successful and significant achievement implemented within the framework of the “alloy/de-alloy” approach is the work of scientists from the Argonne National Research Laboratory, USA, in which framework Pt₃Ni NPs with high catalytic activity in the ORR were obtained from the original octahedral PtNi₃ NPs [129,130]. Initially, the authors obtained NPs of the PtNi₃ alloy. The formed nanocrystals had the shape of classical polyhedra, the edges of which are enriched with Ni atoms. Then, alternating certain methods of heat and acid treatment, the researchers dissolved the “excess” nickel from the NPs body, from which only the framework remained. The former edges of the crystals forming this framework had a Pt₃Ni composition, in which the platinum atoms were segregated mainly on the surface of the nanoframework particles and protected the “internal” nickel atoms from dissolution in the electrolyte. The edges of nanocrystals contain much more active centers per unit surface than the faces. As a result, the electrocatalytic mass activity of actually hollow framework NPs in the ORR was about three times higher than that activity of ordinary platinum NPs. The stability of such NPs, according to the authors of [131], also turned out to be very high. However, according to an authoritative review (article) [132], the commercial use of such catalysts seems to be problematic, due to the complexity of scaling the multi-stage process.

5. Conclusions

Based on the results of the publications analysis, it can be concluded that the chemical or electrochemical activation of bimetallic catalysts has a significant effect on their composition, microstructure, and catalytic activity in the ORR. At the same time, there is no clear understanding of the corrosion conditions influence on the composition and architecture of bimetallic NPs smaller than 5 nm. Studies devoted to establishing the effect of the electrochemical activation conditions on the subsequent behavior of bimetallic catalysts and, in particular, on their activity in the ORR, are fragmentary. The review found that the optimal conditions for acid treatment, in terms of increasing activity in the ORR, is exposure to dilute nitric acid. Note that the electrochemical activation of bimetallic platinum-based catalysts has a greater effect on the ORR activity, compared with treatment in various acids. The stage of electrochemical activation is recommended for use as a mandatory catalyst pre-treatment to obtain highly active de-alloyed materials. Nevertheless, the problems of scaling up the electrochemical treatment of catalysts for commercial applications of such materials remain unresolved.

The analysis of publications data on the heat treatment of platinum-containing catalysts showed that the choice of optimal heat treatment conditions directly depends on the alloying component nature. Thus, higher temperatures (≥ 700 °C) are preferred for treating PtCo/C catalysts, in contrast to PtNi/C materials, for which it is not recommended to use treatment temperatures above 300 °C due to the metal segregation. At that time, for PtCu/C catalysts, there are very big disagreements in the publications about the optimal treatment temperature, which depends on the bimetallic nanoparticles composition.

One of the promising types of catalysts pre-treatment is a combination of acid and heat treatment, which can significantly increase the activity of materials.

Author Contributions: Conceptualization, S.B. and A.A.; methodology, S.B.; formal analysis, A.P. and A.N.; data curation, A.P. and A.N.; writing—original draft preparation, S.B. and A.A.; writing—review and editing, A.P., A.N. and A.A.; visualization, M.D.; supervision, S.B.; project administration, S.B. All authors have read and agreed to the published version of the manuscript.

Funding: This research was financially supported by the Ministry of Science and Higher Education of the Russian Federation (State assignment in the field of scientific activity No 0852-2020-0019).

Institutional Review Board Statement: Not applicable.

Informed Consent Statement: Not applicable.

Data Availability Statement: Not applicable.

Acknowledgments: The authors are grateful to Tabachkova N.Y. The authors appreciate the support from LLC “PROMETHEUS R&D” (Rostov-on-Don), “Shared Use Center “High-Resolution Transmission Electron Microscopy” (SFedU) and LLC “Systems for Microscopy and Analysis” (Skolkovo, Moscow) in conducting the TEM and EDX studies. We would like to acknowledge the Southern Federal University Strategic Academic Leadership Program (“Priority 2030”) for the support of graduate students having taking part in this study.

Conflicts of Interest: The authors declare no conflict of interest.

Abbreviations

FC	Fuel cells
PEMFC	Proton exchange membrane fuel cells
MEA	Membrane-electrode assembly
CV	Cyclic voltammogram
ESA	Electrochemically active surface area
ORR	Oxygen reduction reaction
RHE	Reversible hydrogen electrode
ICP	Inductively Coupled Plasma
EDX	Energy dispersive X-ray
HAADF STEM	High-angle annular dark-field scanning transmission electron microscopy
XRD	X-ray diffraction
XPS	X-ray photoelectron spectroscopy
TEM	Transmission electron microscopy
FCC	Face centered cubic
FCT	Face centered tetragonal
BCC	Body-centered cubic
HSAC	High surface area carbon
EXAFS	Extended X-ray absorption fine structure
FCNTs	Functionalized multi-walled carbon nanotubes

References

- Kongkanand, A.; Mathias, M.F. the priority and challenge of high-power performance of low-platinum proton-exchange membrane fuel cells. *J. Phys. Chem. Lett.* **2016**, *7*, 1127–1137. [[CrossRef](#)] [[PubMed](#)]
- Chan, S.; Jankovic, J.; Susac, D.; Saha, M.S.; Tam, M.; Yang, H.; Ko, F. Electrospun carbon nanofiber catalyst layers for polymer electrolyte membrane fuel cells: Fabrication and optimization. *J. Mater. Sci.* **2018**, *53*, 11633–11647. [[CrossRef](#)]
- Wang, X.X.; Swihart, M.T.; Wu, G. Achievements, challenges and perspectives on cathode catalysts in proton exchange membrane fuel cells for transportation. *Nat. Catal.* **2019**, *2*, 578–589. [[CrossRef](#)]
- Yan, W.; Zhang, D.; Zhang, Q.; Sun, Y.; Zhang, S.; Du, F.; Jin, X. Synthesis of PtCu-based nanocatalysts: Fundamentals and emerging challenges in energy conversion. *J. Energy Chem.* **2022**, *64*, 583–606. [[CrossRef](#)]
- Wang, C.; Spendelow, J.S. recent developments in Pt–Co catalysts for proton-exchange membrane fuel cells. *Curr. Opin. Electrochem.* **2021**, *28*, 100715. [[CrossRef](#)]
- Wang, R.; Wang, H.; Luo, F.; Liao, S. Core-shell-structured low-platinum electrocatalysts for fuel cell applications. *Electrochem. Energy Rev.* **2018**, *1*, 324–387. [[CrossRef](#)]
- Yaroslavtsev, A.B.; Dobrovolsky, Y.A.; Shaglaeva, N.S.; Frolova, L.A.; Gerasimova, E.V.; Sanginov, E.A. Nanostructured materials for low-temperature fuel cells. *Russ. Chem. Rev.* **2012**, *81*, 191–220. [[CrossRef](#)]
- Sui, S.; Wang, X.; Zhou, X.; Su, Y.; Riffat, S.; Liu, C. a comprehensive review of pt electrocatalysts for the oxygen reduction reaction: Nanostructure, activity, mechanism and carbon support in PEM fuel cells. *J. Mater. Chem. A* **2017**, *5*, 1808–1825. [[CrossRef](#)]
- Zaman, S.; Huang, L.; Douka, A.I.; Yang, H.; You, B.; Xia, B.Y. Oxygen reduction electrocatalysts toward practical fuel cells: Progress and perspectives. *Angew. Chem. Int. Ed.* **2021**, *60*, 17832–17852. [[CrossRef](#)]
- Strasser, P. Free electrons to molecular bonds and back: Closing the energetic oxygen reduction (ORR)–Oxygen evolution (OER) cycle using core–Shell Nanoelectrocatalysts. *Acc. Chem. Res.* **2016**, *49*, 2658–2668. [[CrossRef](#)]
- Chaudhari, N.K.; Hong, Y.; Kim, B.; Choi, S.-I.; Lee, K. Pt–Cu based nanocrystals as promising catalysts for various electrocatalytic reactions. *J. Mater. Chem. A* **2019**, *7*, 17183–17203. [[CrossRef](#)]

12. Hussain, S.; Erikson, H.; Kongi, N.; Sarapuu, A.; Solla-Gullón, J.; Maia, G.; Kannan, A.M.; Alonso-Vante, N.; Tammeveski, K. Oxygen reduction reaction on nanostructured pt-based electrocatalysts: A review. *Int. J. Hydrogen Energy* **2020**, *45*, 31775–31797. [[CrossRef](#)]
13. Mølmen, L.; Eiler, K.; Fast, L.; Leisner, P.; Pellicer, E. Recent advances in catalyst materials for proton exchange membrane fuel cells. *APL Mater.* **2021**, *9*, 040702. [[CrossRef](#)]
14. Zhu, F.; Wu, A.; Luo, L.; Wang, C.; Yang, F.; Wei, G.; Xia, G.; Yin, J.; Zhang, J. The asymmetric effects of Cu²⁺ contamination in a proton exchange membrane fuel cell (PEMFC). *Fuel Cells* **2020**, *20*, 196–202. [[CrossRef](#)]
15. Moriau, L.J.; Hrnjić, A.; Pavličić, A.; Kamšek, A.R.; Petek, U.; Ruiz-Zepeda, F.; Šala, M.; Pavko, L.; Šelih, V.S.; Bele, M.; et al. Resolving the nanoparticles' structure-property relationships at the atomic level: A study of pt-based electrocatalysts. *iScience* **2021**, *24*, 102102. [[CrossRef](#)] [[PubMed](#)]
16. Shao, M.; Chang, Q.; Dodelet, J.-P.; Chenitz, R. Recent advances in electrocatalysts for oxygen reduction reaction. *Chem. Rev.* **2016**, *116*, 3594–3657. [[CrossRef](#)] [[PubMed](#)]
17. Kuna, E.; Mrdenovic, D.; Jönsson-Niedziółka, M.; Pieta, P.; Pieta, I.S. Bimetallic nanocatalysts supported on graphitic carbon nitride for sustainable energy development: The shape-structure-activity relation. *Nanoscale Adv.* **2021**, *3*, 1342–1351. [[CrossRef](#)]
18. Lyu, X.; Jia, Y.; Mao, X.; Li, D.; Li, G.; Zhuang, L.; Wang, X.; Yang, D.; Wang, Q.; Du, A.; et al. Gradient-concentration design of stable core-shell nanostructure for acidic oxygen reduction electrocatalysis. *Adv. Mater.* **2020**, *32*, 2003493. [[CrossRef](#)]
19. Alekseenko, A.A.; Guterman, V.E.; Belenov, S.V.; Menshikov, V.S.; Tabachkova, N.Y.; Safronenko, O.I.; Moguchikh, E.A. Pt/C electrocatalysts based on the nanoparticles with the gradient structure. *Int. J. Hydrogen Energy* **2018**, *43*, 3676–3687. [[CrossRef](#)]
20. Lim, T.; Kim, O.-H.; Sung, Y.-E.; Kim, H.-J.; Lee, H.-N.; Cho, Y.-H.; Kwon, O.J. Preparation of onion-like Pt-terminated Pt-Cu bimetallic nano-sized electrocatalysts for oxygen reduction reaction in fuel cells. *J. Power Sources* **2016**, *316*, 124–131. [[CrossRef](#)]
21. Herron, J.A.; Jiao, J.; Hahn, K.; Peng, G.; Adzic, R.R.; Mavrikakis, M. Oxygen reduction reaction on platinum-terminated “onion-structured” alloy catalysts. *Electrocatalysis* **2012**, *3*, 192–202. [[CrossRef](#)]
22. Ge, X.; Chen, L.; Kang, J.; Fujita, T.; Hirata, A.; Zhang, W.; Jiang, J.; Chen, M. A core-shell nanoporous Pt-Cu catalyst with tunable composition and high catalytic activity. *Adv. Funct. Mater.* **2013**, *23*, 4156–4162. [[CrossRef](#)]
23. Luo, M.; Wei, L.; Wang, F.; Han, K.; Zhu, H. Gram-level synthesis of core-shell structured catalysts for the oxygen reduction reaction in proton exchange membrane fuel cells. *J. Power Sources* **2014**, *270*, 34–41. [[CrossRef](#)]
24. Chandran, R.; Dharmalingam, S. Facile synthesis and characterization of PtCu core-shell and alloy nanoparticles. *J. Nanosci. Nanotechnol.* **2014**, *14*, 6957–6964. [[CrossRef](#)] [[PubMed](#)]
25. Alekseenko, A.A.; Belenov, S.V.; Menshikov, V.S.; Guterman, V.E. Pt(Cu)/C electrocatalysts with low platinum content. *Russ. J. Electrochem.* **2018**, *54*, 415–425. [[CrossRef](#)]
26. Guterman, V.E.; Belenov, S.V.; Pakharev, A.Y.; Min, M.; Tabachkova, N.Y.; Mikheykina, E.B.; Vysochina, L.L.; Lastovina, T.A. Pt-M/C (M = Cu, Ag) electrocatalysts with an inhomogeneous distribution of metals in the nanoparticles. *Int. J. Hydrogen Energy* **2016**, *41*, 1609–1626. [[CrossRef](#)]
27. Sarkar, A.; Manthiram, A. Synthesis of Pt@Cu core-shell nanoparticles by galvanic displacement of Cu by Pt⁴⁺ ions and their application as electrocatalysts for oxygen reduction reaction in fuel cells. *J. Phys. Chem. C* **2010**, *114*, 4725–4732. [[CrossRef](#)]
28. Xiao, F.; Wang, Y.; Wu, Z.; Chen, G.; Yang, F.; Zhu, S.; Siddharth, K.; Kong, Z.; Lu, A.; Li, J.; et al. Recent advances in electrocatalysts for proton exchange membrane fuel cells and alkaline membrane fuel cells. *Adv. Mater.* **2021**, *33*, 2006292. [[CrossRef](#)]
29. Bezerra, C.W.B.; Zhang, L.; Liu, H.; Lee, K.; Marques, A.L.B.; Marques, E.P.; Wang, H.; Zhang, J. A review of heat-treatment effects on activity and stability of PEM fuel cell catalysts for oxygen reduction reaction. *J. Power Sources* **2007**, *173*, 891–908. [[CrossRef](#)]
30. Sang, Q.; Hao, S.; Han, J.; Ding, Y. Dealloyed nanoporous materials for electrochemical energy conversion and storage. *EnergyChem* **2022**, *4*, 100069. [[CrossRef](#)]
31. Weissmüller, J.; Sieradzki, K. Dealloyed nanoporous materials with interface-controlled behavior. *MRS Bull.* **2018**, *43*, 14–19. [[CrossRef](#)]
32. Guo, N.; Xue, H.; Bao, A.; Wang, Z.; Sun, J.; Song, T.; Ge, X.; Zhang, W.; Huang, K.; He, F.; et al. Achieving superior electrocatalytic performance by surface copper vacancy defects during electrochemical etching process. *Angew. Chem. Int. Ed.* **2020**, *59*, 13778–13784. [[CrossRef](#)] [[PubMed](#)]
33. Dutta, I.; Carpenter, M.K.; Balogh, M.P.; Ziegelbauer, J.M.; Moylan, T.E.; Atwan, M.H.; Irish, N.P. Electrochemical and structural study of a chemically dealloyed PtCu oxygen reduction catalyst. *J. Phys. Chem. C* **2010**, *114*, 16309–16320. [[CrossRef](#)] [[PubMed](#)]
34. Sohn, Y.; Park, J.H.; Kim, P.; Joo, J.B. Dealloyed PtCu catalyst as an efficient electrocatalyst in oxygen reduction reaction. *Curr. Appl. Phys.* **2015**, *15*, 993–999. [[CrossRef](#)]
35. Gan, L.; Yu, R.; Luo, J.; Cheng, Z.; Zhu, J. Lattice strain distributions in individual dealloyed Pt-Fe catalyst nanoparticles. *J. Phys. Chem. Lett.* **2012**, *3*, 934–938. [[CrossRef](#)]
36. Kirakosyan, S.A.; Alekseenko, A.A.; Guterman, V.E.; Novomlinskii, I.N.; Men'shchikov, V.S.; Gerasimova, E.V.; Nikulin, A.Y. De-Alloyed PtCu/C Catalysts of Oxygen Electroreduction. *Russ. J. Electrochem.* **2019**, *55*, 1258–1268. [[CrossRef](#)]
37. Jung, J.Y.; Kim, D.; Jang, I.; Kim, N.D.; Yoo, S.J.; Kim, P. Synthesis of hollow structured PtNi/Pt core/shell and Pt-Only nanoparticles via galvanic displacement and selective etching for efficient oxygen reduction reaction. *J. Ind. Eng. Chem.* **2022**. [[CrossRef](#)]
38. Wu, Y.; Wang, D.; Niu, Z.; Chen, P.; Zhou, G.; Li, Y. A strategy for designing a concave Pt-Ni Alloy through controllable chemical etching. *Angew. Chem. Int. Ed.* **2012**, *51*, 12524–12528. [[CrossRef](#)]

39. Gan, L.; Heggen, M.; O'Malley, R.; Theobald, B.; Strasser, P. Understanding and controlling nanoporosity formation for improving the stability of bimetallic fuel cell catalysts. *Nano Lett.* **2013**, *13*, 1131–1138. [[CrossRef](#)]
40. Gatalo, M.; Moriau, L.; Petek, U.; Ruiz-Zepeda, F.; Šala, M.; Grom, M.; Galun, T.; Jovanović, P.; Pavlišič, A.; Bele, M.; et al. CO-assisted ex-situ chemical activation of Pt-Cu/C oxygen reduction reaction electrocatalyst. *Electrochim. Acta* **2019**, *306*, 377–386. [[CrossRef](#)]
41. Wang, D.; Zhao, P.; Li, Y. General preparation for Pt-Based alloy nanoporous nanoparticles as potential nanocatalysts. *Sci. Rep.* **2011**, *1*, 37. [[CrossRef](#)] [[PubMed](#)]
42. Dubau, L.; Lopez-Haro, M.; Durst, J.; Maillard, F. Atomic-scale restructuring of hollow PtNi/C electrocatalysts during accelerated stress tests. *Catal. Today* **2016**, *262*, 146–154. [[CrossRef](#)]
43. Lopez-Haro, M.; Dubau, L.; Guétaz, L.; Bayle-Guillemaud, P.; Chatenet, M.; André, J.; Caqué, N.; Rossinot, E.; Maillard, F. Atomic-scale structure and composition of Pt₃Co/C nanocrystallites during real pemfc operation: A STEM-EELS study. *Appl. Catal. B Environ.* **2014**, *152–153*, 300–308. [[CrossRef](#)]
44. Menshchikov, V.; Alekseenko, A.; Guterman, V.; Nechitailov, A.; Glebova, N.; Tomasov, A.; Spiridonova, O.; Belenov, S.; Zelenina, N.; Safronenko, O. Effective platinum-copper catalysts for methanol oxidation and oxygen reduction in proton-exchange membrane fuel cell. *Nanomaterials* **2020**, *10*, 742. [[CrossRef](#)]
45. Pavlets, A.; Alekseenko, A.; Nikulin, A. Influence of acid treatment on the functional characteristics of PtCu/C electrocatalysts. In *Springer Proceedings in Materials*; Springer: Cham, Switzerland, 2021; Volume 10, pp. 25–35. [[CrossRef](#)]
46. Koh, S.; Strasser, P. Electrocatalysis on bimetallic surfaces: Modifying catalytic reactivity for oxygen reduction by voltammetric surface dealloying. *J. Am. Chem. Soc.* **2007**, *129*, 12624–12625. [[CrossRef](#)]
47. Mani, P.; Srivastava, R.; Yu, C.; Strasser, P. In-situ, In-layer De-alloying of Pt-M intermetallics for high performance PEMFC electrode layers: Mea activity and durability studies. *ECS Trans.* **2007**, *11*, 933–939. [[CrossRef](#)]
48. Strasser, P.; Koh, S.; Anniyev, T.; Greeley, J.; More, K.; Yu, C.; Liu, Z.; Kaya, S.; Nordlund, D.; Ogasawara, H.; et al. Lattice-strain control of the activity in dealloyed core-shell fuel cell catalysts. *Nat. Chem.* **2010**, *2*, 454–460. [[CrossRef](#)]
49. Neyerlin, K.C.; Srivastava, R.; Yu, C.; Strasser, P. Electrochemical activity and stability of dealloyed Pt–Cu and Pt–Cu–Co electrocatalysts for the oxygen reduction reaction (ORR). *J. Power Sources* **2009**, *186*, 261–267. [[CrossRef](#)]
50. Mani, P.; Srivastava, R.; Strasser, P. Dealloyed Pt–Cu core–shell nanoparticle electrocatalysts for use in PEM fuel cell cathodes. *J. Phys. Chem. C* **2008**, *112*, 2770–2778. [[CrossRef](#)]
51. Gatalo, M.; Jovanović, P.; Ruiz-Zepeda, F.; Pavlišič, A.; Robba, A.; Bale, M.; Dražič, G.; Gaberšček, M.; Hodnik, N. Insights into electrochemical dealloying of Cu out of Au-doped Pt-alloy nanoparticles at the sub-nano-scale. *J. Electrochem. Sci. Eng.* **2018**, *8*, 87–100. [[CrossRef](#)]
52. Barim, S.B.; Bozbag, S.E.; Deljoo, B.; Aindow, M.; Erkey, C. Highly active carbon supported PtCu electrocatalysts for PEMFCs by *in Situ* supercritical deposition coupled with electrochemical dealloying. *Fuel Cells* **2020**, *20*, 285–299. [[CrossRef](#)]
53. Baldizzone, C.; Gan, L.; Hodnik, N.; Keeley, G.P.; Kostka, A.; Heggen, M.; Strasser, P.; Mayrhofer, K.J.J. Stability of dealloyed porous Pt/Ni nanoparticles. *ACS Catal.* **2015**, *5*, 5000–5007. [[CrossRef](#)]
54. Snyder, J.; McCue, I.; Livi, K.; Erlebacher, J. Structure/processing/properties relationships in nanoporous nanoparticles as applied to catalysis of the cathodic oxygen reduction reaction. *J. Am. Chem. Soc.* **2012**, *134*, 8633–8645. [[CrossRef](#)] [[PubMed](#)]
55. Jeyabharathi, C.; Hodnik, N.; Baldizzone, C.; Meier, J.C.; Heggen, M.; Phani, K.L.N.; Bele, M.; Zorko, M.; Hocevar, S.; Mayrhofer, K.J.J. Time evolution of the stability and oxygen reduction reaction activity of PtCu/C nanoparticles. *ChemCatChem* **2013**, *5*, 2627–2635. [[CrossRef](#)]
56. Yang, T.; Pukazhselvan, D.; da Silva, E.L.; Santos, M.C.; Meng, L.; Ramasamy, D.; Jothi, S.; Graça, V.; Shi, S. Highly branched Pt Cu nanodandelion with high activity for oxygen reduction reaction. *Int. J. Hydrogen Energy* **2019**, *44*, 174–179. [[CrossRef](#)]
57. Wang, D.; Yu, Y.; Xin, H.L.; Hovden, R.; Ercius, P.; Mundy, J.A.; Chen, H.; Richard, J.H.; Muller, D.A.; DiSalvo, F.J.; et al. Tuning oxygen reduction reaction activity via controllable dealloying: A model study of ordered Cu₃Pt/C intermetallic nanocatalysts. *Nano Lett.* **2012**, *12*, 5230–5238. [[CrossRef](#)]
58. Garcia-Cardona, J.; Sirés, I.; Alcaide, F.; Brillas, E.; Centellas, F.; Cabot, P.L. Electrochemical performance of carbon-supported Pt(Cu) electrocatalysts for low-temperature fuel cells. *Int. J. Hydrogen Energy* **2020**, *45*, 20582–20593. [[CrossRef](#)]
59. Oezaslan, M.; Heggen, M.; Strasser, P. Size-dependent morphology of dealloyed bimetallic catalysts: Linking the nano to the macro scale. *J. Am. Chem. Soc.* **2012**, *134*, 514–524. [[CrossRef](#)]
60. Ruiz-Zepeda, F.; Gatalo, M.; Pavlišič, A.; Dražič, G.; Jovanović, P.; Bele, M.; Gaberšček, M.; Hodnik, N. Atomically resolved anisotropic electrochemical shaping of nano-electrocatalyst. *Nano Lett.* **2019**, *19*, 4919–4927. [[CrossRef](#)]
61. Pavlets, A.; Alekseenko, A.; Menshchikov, V.; Belenov, S.; Volochaev, V.; Pankov, I.; Safronenko, O.; Guterman, V. Influence of electrochemical pretreatment conditions of PtCu/C alloy electrocatalyst on its activity. *Nanomaterials* **2021**, *11*, 1499. [[CrossRef](#)]
62. Alekseenko, A.A.; Pavlets, A.S.; Belenov, S.V.; Safronenko, O.I.; Pankov, I.V.; Guterman, V.E. The electrochemical activation mode as a way to exceptional ORR performance of nanostructured PtCu/C materials. *Appl. Surf. Sci.* **2022**, *595*, 153533. [[CrossRef](#)]
63. Cai, X.; Lin, R.; Shen, D.; Zhu, Y. Gram-scale synthesis of well-dispersed shape-controlled Pt–Ni/C as high-performance catalysts for the oxygen reduction reaction. *ACS Appl. Mater. Interfaces* **2019**, *11*, 29689–29697. [[CrossRef](#)]
64. Niu, H.-J.; Chen, H.-Y.; Wen, G.-L.; Feng, J.-J.; Zhang, Q.-L.; Wang, A.-J. One-pot solvothermal synthesis of three-dimensional hollow PtCu alloyed dodecahedron nanoframes with excellent electrocatalytic performances for hydrogen evolution and oxygen reduction. *J. Colloid Interface Sci.* **2019**, *539*, 525–532. [[CrossRef](#)]

65. Gatalo, M.; Jovanovič, P.; Petek, U.; Šala, M.; Šelih, V.S.; Ruiz-Zepeda, F.; Bele, M.; Hodnik, N.; Gaberšček, M. Comparison of Pt–Cu/C with benchmark Pt–Co/C: Metal dissolution and their surface interactions. *ACS Appl. Energy Mater.* **2019**, *2*, 3131–3141. [[CrossRef](#)]
66. Cherevko, S.; Kulyk, N.; Mayrhofer, K.J.J. Durability of platinum-based fuel cell electrocatalysts: Dissolution of bulk and nanoscale platinum. *Nano Energy* **2016**, *29*, 275–298. [[CrossRef](#)]
67. Topalov, A.A.; Katsounaros, I.; Auinger, M.; Cherevko, S.; Meier, J.C.; Klemm, S.O.; Mayrhofer, K.J.J. Dissolution of platinum: Limits for the deployment of electrochemical energy conversion? *Angew. Chem. Int. Ed.* **2012**, *51*, 12613–12615. [[CrossRef](#)]
68. Topalov, A.A.; Cherevko, S.; Zeradjanin, A.R.; Meier, J.C.; Katsounaros, I.; Mayrhofer, K.J.J. Towards a comprehensive understanding of platinum dissolution in acidic media. *Chem. Sci.* **2014**, *5*, 631–638. [[CrossRef](#)]
69. Wu, Z.-P.; Caracciolo, D.T.; Maswadeh, Y.; Wen, J.; Kong, Z.; Shan, S.; Vargas, J.A.; Yan, S.; Hopkins, E.; Park, K.; et al. Alloying–realloying enabled high durability for Pt–Pd–3d-transition metal nanoparticle fuel cell catalysts. *Nat. Commun.* **2021**, *12*, 859. [[CrossRef](#)]
70. Cui, Y.; Wu, Y.; Wang, Z.; Yao, X.; Wei, Y.; Kang, Y.; Du, H.; Li, J.; Gan, L. Mitigating metal dissolution and redeposition of Pt–Co catalysts in PEM fuel cells: Impacts of structural ordering and particle size. *J. Electrochem. Soc.* **2020**, *167*, 064520. [[CrossRef](#)]
71. Wu, Z.-P.; Shan, S.; Zang, S.-Q.; Zhong, C.-J. Dynamic core–shell and alloy structures of multimetallic nanomaterials and their catalytic synergies. *Acc. Chem. Res.* **2020**, *53*, 2913–2924. [[CrossRef](#)]
72. Oezaslan, M.; Hasché, F.; Strasser, P. PtCu₃, PtCu and Pt₃Cu alloy nanoparticle electrocatalysts for oxygen reduction reaction in alkaline and acidic media. *J. Electrochem. Soc.* **2012**, *159*, B444–B454. [[CrossRef](#)]
73. Yang, W.; Zou, L.; Huang, Q.; Zou, Z.; Hu, Y.; Yang, H. Lattice contracted ordered intermetallic core-shell PtCo@Pt nanoparticles: Synthesis, structure and origin for enhanced oxygen reduction reaction. *J. Electrochem. Soc.* **2017**, *164*, H331–H337. [[CrossRef](#)]
74. Su, Y.; Feng, M.; Zhang, C.; Yan, Z.; Liu, H.; Tang, J.; Du, H. Platinum nanowires: Structural and catalytic evolution upon annealing temperature. *Electrochim. Acta* **2015**, *164*, 182–186. [[CrossRef](#)]
75. Humphrey, J.J.L.; Sadasivan, S.; Plana, D.; Celorrio, V.; Tooze, R.A.; Fermín, D.J. Surface activation of Pt nanoparticles synthesised by “hot injection” in the presence of oleylamine. *Chem. A Eur. J.* **2015**, *21*, 12694–12701. [[CrossRef](#)]
76. Han, K.; Moon, Y.; Han, O.; Hwang, K.; Kim, I.; Kim, H. Heat treatment and potential cycling effects on surface morphology, particle size, and catalytic activity of Pt/C catalysts studied by ¹³C NMR, TEM, XRD and CV. *Electrochem. Commun.* **2007**, *9*, 317–324. [[CrossRef](#)]
77. Hasché, F.; Oezaslan, M.; Strasser, P. In situ observation of the thermally induced growth of platinum-nanoparticle catalysts using high-temperature X-Ray diffraction. *ChemPhysChem* **2012**, *13*, 828–834. [[CrossRef](#)]
78. Chung, D.Y.; Chung, Y.-H.; Jung, N.; Choi, K.-H.; Sung, Y.-E. Correlation between platinum nanoparticle surface rearrangement induced by heat treatment and activity for an oxygen reduction reaction. *Phys. Chem. Chem. Phys.* **2013**, *15*, 13658. [[CrossRef](#)]
79. Wettergren, K.; Schweinberger, F.F.; Deiana, D.; Ridge, C.J.; Crampton, A.S.; Rötzer, M.D.; Hansen, T.W.; Zhdanov, V.P.; Heiz, U.; Langhammer, C. High sintering resistance of size-selected platinum cluster catalysts by suppressed ostwald ripening. *Nano Lett.* **2014**, *14*, 5803–5809. [[CrossRef](#)]
80. Jeon, M.K.; Zhang, Y.; McGinn, P.J. A comparative study of PtCo, PtCr, and PtCoCr catalysts for oxygen electro-reduction reaction. *Electrochim. Acta* **2010**, *55*, 5318–5325. [[CrossRef](#)]
81. Kang, Y.S.; Yoo, S.J.; Lee, M.J.; Kim, M.-J.; Lee, S.Y.; Lee, K.-S.; Sung, Y.-E. Facile synthesis of platinum alloy electrocatalyst via aluminum reducing agent and the effect of post heat treatment for oxygen reduction reaction. *Int. J. Hydrogen Energy* **2016**, *41*, 22952–22962. [[CrossRef](#)]
82. Jung, W.S.; Lee, J. Induced changes of Pt/C in activity and durability through heat-treatment for oxygen reduction reaction in acidic medium. *Int. J. Hydrogen Energy* **2017**, *42*, 22830–22840. [[CrossRef](#)]
83. Liu, Z.; Yu, C.; Rusakova, I.A.; Huang, D.; Strasser, P. Synthesis of Pt₃Co alloy nanocatalyst via reverse micelle for oxygen reduction reaction in PEMFCs. *Top. Catal.* **2008**, *49*, 241–250. [[CrossRef](#)]
84. Valisi, A.N.; Maiyalagan, T.; Khotseng, L.; Linkov, V.; Pasupathi, S. Effects of heat treatment on the catalytic activity and methanol tolerance of carbon-supported platinum alloys. *Electrocatalysis* **2012**, *3*, 108–118. [[CrossRef](#)]
85. Jung, C.; Lee, C.; Bang, K.; Lim, J.; Lee, H.; Ryu, H.J.; Cho, E.; Lee, H.M. Synthesis of chemically ordered Pt₃Fe/C intermetallic electrocatalysts for oxygen reduction reaction with enhanced activity and durability via a removable carbon coating. *ACS Appl. Mater. Interfaces* **2017**, *9*, 31806–31815. [[CrossRef](#)]
86. Zamanzad Ghavidel, M.R.; Monteverde Videla, A.H.A.; Specchia, S.; Easton, E.B. The relationship between the structure and ethanol oxidation activity of Pt–Cu/C alloy catalysts. *Electrochim. Acta* **2017**, *230*, 58–72. [[CrossRef](#)]
87. Pryadchenko, V.V.; Belenov, S.V.; Shemet, D.B.; Srabionyan, V.V.; Avakyan, L.A.; Volochaev, V.A.; Mikheykin, A.S.; Bdoyan, K.E.; Zizak, I.; Guterman, V.E.; et al. Effect of thermal treatment on the atomic structure and electrochemical characteristics of bimetallic PtCu core–shell nanoparticles in PtCu/C electrocatalysts. *J. Phys. Chem. C* **2018**, *122*, 17199–17210. [[CrossRef](#)]
88. Pryadchenko, V.V.; Belenov, S.V.; Shemet, D.B.; Volochaev, V.A.; Srabionyan, V.V.; Avakyan, L.A.; Tabachkova, N.Y.; Guterman, V.E.; Bugaev, L.A. The effect of thermal treatment on the atomic structure of core–shell PtCu nanoparticles in PtCu/C electrocatalysts. *Phys. Solid State* **2017**, *59*, 1666–1673. [[CrossRef](#)]
89. Belenov, S.V.; Menshikov, V.S.; Nevelskaya, A.K.; Rezvan, D.V. Influence of PtCuAu’s nanoparticle structure on its activity in methanol oxidation reaction. *Nanotechnol Russ* **2019**, *14*, 557–564. [[CrossRef](#)]

90. Mauer, D.; Belenov, S.; Guterman, V.; Nikolsky, A.; Kozakov, A.; Nikulin, A.; Alexeenko, D.; Safronenko, O. Gram-scale synthesis of CoO/C as base for PtCo/C high-performance catalysts for the oxygen reduction reaction. *Catalysts* **2021**, *11*, 1539. [[CrossRef](#)]
91. Konno, N.; Mizuno, S.; Nakaji, H.; Ishikawa, Y. Development of compact and high-performance fuel cell stack. *SAE Int. J. Altern. Powertrains* **2015**, *4*, 2015-01-1175. [[CrossRef](#)]
92. Lin, R.; Cao, C.; Zhao, T.; Huang, Z.; Li, B.; Wieckowski, A.; Ma, J. Synthesis and application of core-shell Co@Pt/C electrocatalysts for proton exchange membrane fuel cells. *J. Power Sources* **2013**, *223*, 190–198. [[CrossRef](#)]
93. Lin, R.; Zhao, T.; Shang, M.; Wang, J.; Tang, W.; Guterman, V.E.; Ma, J. Effect of heat treatment on the activity and stability of PtCo/C catalyst and application of in-Situ X-Ray absorption near edge structure for proton exchange membrane fuel cell. *J. Power Sources* **2015**, *293*, 274–282. [[CrossRef](#)]
94. Oezaslan, M.; Strasser, P. Activity of dealloyed PtCo₃ and PtCu₃ nanoparticle electrocatalyst for oxygen reduction reaction in polymer electrolyte membrane fuel cell. *J. Power Sources* **2011**, *196*, 5240–5249. [[CrossRef](#)]
95. Wang, D.; Xin, H.L.; Hovden, R.; Wang, H.; Yu, Y.; Muller, D.A.; DiSalvo, F.J.; Abruña, H.D. Structurally ordered intermetallic platinum–cobalt core–shell nanoparticles with enhanced activity and stability as oxygen reduction electrocatalysts. *Nat. Mater.* **2013**, *12*, 81–87. [[CrossRef](#)]
96. Zhao, Q.; Wang, C.; Wang, H.; Wang, J.; Tang, Y.; Mao, Z.; Sasaki, K. H₂-induced thermal treatment significantly influences the development of a high performance low-platinum core-shell PtNi/C alloyed oxygen reduction catalyst. *Int. J. Energy Res.* **2020**, *44*, 4773–4783. [[CrossRef](#)]
97. Beermann, V.; Gocyla, M.; Kühn, S.; Padgett, E.; Schmies, H.; Goerlin, M.; Erini, N.; Shviro, M.; Heggen, M.; Dunin-Borkowski, R.E.; et al. Tuning the electrocatalytic oxygen reduction reaction activity and stability of shape-controlled Pt–Ni nanoparticles by thermal annealing—Elucidating the surface atomic structural and compositional changes. *J. Am. Chem. Soc.* **2017**, *139*, 16536–16547. [[CrossRef](#)]
98. El-Deeb, H.; Bron, M. Microwave-assisted polyol synthesis of PtCu/carbon nanotube catalysts for electrocatalytic oxygen reduction. *J. Power Sources* **2015**, *275*, 893–900. [[CrossRef](#)]
99. Jung, W.S.; Popov, B.N. Effect of pretreatment on durability of Fct-structured Pt-based alloy catalyst for the oxygen reduction reaction under operating conditions in polymer electrolyte membrane fuel cells. *ACS Sustain. Chem. Eng.* **2017**, *5*, 9809–9817. [[CrossRef](#)]
100. Kang, Y.S.; Choi, K.-H.; Ahn, D.; Lee, M.J.; Baik, J.; Chung, D.Y.; Kim, M.-J.; Lee, S.Y.; Kim, M.; Shin, H.; et al. Effect of post heat-treatment of composition-controlled PdFe nanoparticles for oxygen reduction reaction. *J. Power Sources* **2016**, *303*, 234–242. [[CrossRef](#)]
101. Mai, Y.; Xie, X.; Wang, Z.; Yan, C.; Liu, G. Effect of heat treatment temperature on the Pt₃Co binary metal catalysts for oxygen reduced reaction and DFT calculations. *J. Fuel Chem. Technol.* **2022**, *50*, 114–121. [[CrossRef](#)]
102. Wen, Y.-H.; Zhang, L.-H.; Wang, J.-B.; Huang, R. Atomic-scale insights into thermal stability of Pt₃Co nanoparticles: A comparison between disordered alloy and ordered intermetallics. *J. Alloys Compd.* **2019**, *776*, 629–635. [[CrossRef](#)]
103. Nassr, A.B.A.A.; Sinev, I.; Grünert, W.; Bron, M. PtNi supported on oxygen functionalized carbon nanotubes: In depth structural characterization and activity for methanol electrooxidation. *Appl. Catal. B Environ.* **2013**, *142–143*, 849–860. [[CrossRef](#)]
104. Liao, M.; Li, W.; Peng, J.; Zhang, F.; Xu, W.; Huang, Z. Enhancement of anodic oxidation of formic acid on Pd–Fe bimetallic nanoparticles by thermal treatment. *Int. J. Hydrogen Energy* **2021**, *46*, 10239–10246. [[CrossRef](#)]
105. Gocyla, M.; Kuehl, S.; Shviro, M.; Heyen, H.; Selve, S.; Dunin-Borkowski, R.E.; Heggen, M.; Strasser, P. Shape stability of octahedral PtNi nanocatalysts for electrochemical oxygen reduction reaction studied by *in Situ* transmission electron microscopy. *ACS Nano* **2018**, *12*, 5306–5311. [[CrossRef](#)] [[PubMed](#)]
106. Xiao, F.; Qin, X.; Xu, M.; Zhu, S.; Zhang, L.; Hong, Y.; Choi, S.-I.; Chang, Q.; Xu, Y.; Pan, X.; et al. Impact of heat treatment on the electrochemical properties of carbon-supported octahedral Pt–Ni nanoparticles. *ACS Catal.* **2019**, *9*, 11189–11198. [[CrossRef](#)]
107. Ortatatlı, Ş.; Knossalla, J.; Schüth, F.; Weidenthaler, C. Monitoring the formation of PtNi nanoalloys supported on hollow graphitic spheres using *in Situ* Pair distribution function analysis. *Phys. Chem. Chem. Phys.* **2018**, *20*, 8466–8474. [[CrossRef](#)]
108. Cai, X.; Lin, R.; Liu, X.; Zhao, Y. Effect of heat treatment on the surface structure of Pd@Pt–Ni core-shell catalysts for the oxygen reduction reaction. *J. Alloys Compd.* **2021**, *884*, 161059. [[CrossRef](#)]
109. Antolini, E. Alloy vs. intermetallic compounds: Effect of the ordering on the electrocatalytic activity for oxygen reduction and the stability of low temperature fuel cell catalysts. *Appl. Catal. B Environ.* **2017**, *217*, 201–213. [[CrossRef](#)]
110. Hodnik, N.; Jeyabharathi, C.; Meier, J.C.; Kostka, A.; Phani, K.L.; Rečnik, A.; Bele, M.; Hočevár, S.; Gaberšček, M.; Mayrhofer, K.J.J. Effect of ordering of PtCu₃ nanoparticle structure on the activity and stability for the oxygen reduction reaction. *Phys. Chem. Chem. Phys.* **2014**, *16*, 13610–13615. [[CrossRef](#)]
111. Xing, Z.; Li, J.; Wang, S.; Su, C.; Jin, H. Structure engineering of PtCu₃/C catalyst from disordered to ordered intermetallic compound with heat-treatment for the methanol electrooxidation reaction. *Nano Res.* **2022**, *15*, 3866–3871. [[CrossRef](#)]
112. Wu, B.; Du, F.; Wang, H.; Wu, C.; Chu, J.; Wang, X.; Xiong, S. Effects of annealing temperature of PtCu/MWCNT catalysts on their electrocatalytic performance of electrooxidation of methanol. *Ionics* **2022**, *28*, 369–382. [[CrossRef](#)]
113. Babu, P.K.; Kim, H.S.; Kuk, S.T.; Chung, J.H.; Oldfield, E.; Wieckowski, A.; Smotkin, E.S. Activation of nanoparticle Pt–ru fuel cell catalysts by heat treatment: A ¹⁹⁵Pt NMR and electrochemical study. *J. Phys. Chem. B* **2005**, *109*, 17192–17196. [[CrossRef](#)]

114. Gatalo, M.; Ruiz-Zepeda, F.; Hodnik, N.; Dražič, G.; Bele, M.; Gaberšček, M. Insights into thermal annealing of highly-active PtCu₃/C oxygen reduction reaction electrocatalyst: An in-situ heating transmission electron microscopy study. *Nano Energy* **2019**, *63*, 103892. [[CrossRef](#)]
115. Liu, T.; Liu, H.; Ju, F.; Wang, H.; Wang, Y.; Li, W. Carbon-supported Pd–Cr bimetallic nanoparticles and their electrocatalytic activity and durability in oxygen reduction reaction. *Russ. J. Phys. Chem. A* **2017**, *91*, 2283–2287. [[CrossRef](#)]
116. Sahin, N.E.; Napporn, T.W.; Dubau, L.; Kadirgan, F.; Léger, J.-M.; Kokoh, K.B. Temperature-dependence of oxygen reduction activity on Pt/C and PtCr/c electrocatalysts synthesized from microwave-heated diethylene glycol method. *Appl. Catal. B Environ.* **2017**, *203*, 72–84. [[CrossRef](#)]
117. Duan, H.; Xu, C. Nanoporous PdCr alloys as highly active electrocatalysts for oxygen reduction reaction. *Phys. Chem. Chem. Phys.* **2016**, *18*, 4166–4173. [[CrossRef](#)] [[PubMed](#)]
118. Maniwan, W.; Poochinda, K.; Hunsom, M. Activity and stability of PtCr/C catalyst for oxygen reduction reaction: Effect of the Pt:Cr ratio and heat treatment atmosphere. *Int. J. Hydrogen Energy* **2016**, *41*, 21404–21414. [[CrossRef](#)]
119. Kaewsai, D.; Yeamdee, S.; Supajaroen, S.; Hunsom, M. ORR activity and stability of PtCr/C catalysts in a low temperature/pressure PEM fuel cell: Effect of heat treatment temperature. *Int. J. Hydrogen Energy* **2018**, *43*, 5133–5144. [[CrossRef](#)]
120. Min, M.; Kim, H. Performance and stability studies of PtCr/C alloy catalysts for oxygen reduction reaction in low temperature fuel cells. *Int. J. Hydrogen Energy* **2016**, *41*, 17557–17566. [[CrossRef](#)]
121. Tsyppkin, M.; de la Fuente, J.L.G.; García Rodríguez, S.; Yu, Y.; Ochal, P.; Seland, F.; Safonova, O.; Muthuswamy, N.; Rønning, M.; Chen, D.; et al. Effect of heat treatment on the electrocatalytic properties of nano-structured ru cores with Pt shells. *J. Electroanal. Chem.* **2013**, *704*, 57–66. [[CrossRef](#)]
122. Wu, Z.-P.; Shan, S.; Xie, Z.-H.; Kang, N.; Park, K.; Hopkins, E.; Yan, S.; Sharma, A.; Luo, J.; Wang, J.; et al. Revealing the role of phase structures of bimetallic nanocatalysts in the oxygen reduction reaction. *ACS Catal.* **2018**, *8*, 11302–11313. [[CrossRef](#)]
123. Belenov, S.V.; Menshchikov, V.S.; Nevelskaya, A.K.; Pryadchenko, V.V.; Shemet, D.B.; Srabionyan, V.V.; Alekseenko, A.A.; Kirakosyan, S.A.; Guterman, V.E. Post-treatment of Pt-M (M = Cu, Co, Ni)/C electrocatalysts with different distribution of metals in nanoparticles: Evolution of structure and activity. In *Springer Proceedings in Physics*; Springer: Cham, Switzerland, 2017; Volume 207, pp. 65–77. [[CrossRef](#)]
124. Chaisuban, N.; Maniwan, W.; Hunsom, M. Effect of heat-treatment on the performance of PtM/C (M = Cr, Pd, Co) catalysts towards the oxygen reduction reaction in PEM fuel cell. *Energy* **2017**, *127*, 454–461. [[CrossRef](#)]
125. Chen, L.; Zhu, J.; Xuan, C.; Xiao, W.; Xia, K.; Xia, W.; Lai, C.; Xin, H.L.; Wang, D. Effects of crystal phase and composition on structurally ordered Pt–Co–Ni/C ternary intermetallic electrocatalysts for the formic acid oxidation reaction. *J. Mater. Chem. A* **2018**, *6*, 5848–5855. [[CrossRef](#)]
126. Li, B.; Yan, Z.; Xiao, Q.; Dai, J.; Yang, D.; Zhang, C.; Cai, M.; Ma, J. Highly active carbon-supported Pt nanoparticles modified and dealloyed with Co for the oxygen reduction reaction. *J. Power Sources* **2014**, *270*, 201–207. [[CrossRef](#)]
127. Beermann, V.; Köhl, S.; Strasser, P. Tuning the catalytic oxygen reduction reaction performance of Pt–Ni octahedral nanoparticles by acid treatments and thermal annealing. *J. Electrochem. Soc.* **2018**, *165*, J3026–J3030. [[CrossRef](#)]
128. Wang, Y.-J.; Zhao, N.; Fang, B.; Li, H.; Bi, X.T.; Wang, H. A highly efficient PtCo/C electrocatalyst for the oxygen reduction reaction. *RSC Adv.* **2016**, *6*, 34484–34491. [[CrossRef](#)]
129. Becknell, N.; Kang, Y.; Chen, C.; Resasco, J.; Kornienko, N.; Guo, J.; Markovic, N.M.; Somorjai, G.A.; Stamenkovic, V.R.; Yang, P. Atomic structure of Pt₃Ni nanoframe electrocatalysts by *in Situ* X-ray absorption spectroscopy. *J. Am. Chem. Soc.* **2015**, *137*, 15817–15824. [[CrossRef](#)] [[PubMed](#)]
130. Becknell, N.; Son, Y.; Kim, D.; Li, D.; Yu, Y.; Niu, Z.; Lei, T.; Sneed, B.T.; More, K.L.; Markovic, N.M.; et al. Control of architecture in rhombic dodecahedral Pt–Ni nanoframe electrocatalysts. *J. Am. Chem. Soc.* **2017**, *139*, 11678–11681. [[CrossRef](#)] [[PubMed](#)]
131. Chen, C.; Kang, Y.; Huo, Z.; Zhu, Z.; Huang, W.; Xin, H.L.; Snyder, J.D.; Li, D.; Herron, J.A.; Mavrikakis, M.; et al. Highly crystalline multimetallic nanoframes with three-dimensional electrocatalytic surfaces. *Science* **2014**, *343*, 1339–1343. [[CrossRef](#)] [[PubMed](#)]
132. Banham, D.; Ye, S. Current status and future development of catalyst materials and catalyst layers for proton exchange membrane fuel cells: An industrial perspective. *ACS Energy Lett.* **2017**, *2*, 629–638. [[CrossRef](#)]